QUANTUM ENHANCED ELECTRON TRANSFER IN COUPLED PORPHYRINS

by

Andrew Jesse Pedersen

A thesis submitted to the faculty of
The University of North Carolina at Charlotte
In partial fulfillment of the requirements
For the degree of Master of Science in
Chemistry

Charlotte

2015

Approved by:

_____
Dr. Marcus Jones

_____
Dr. Michael Walter

_____
Dr. Thomas Schmedake

_____
Dr. Edward Stokes

ABSTRACT

ANDREW JESSE PEDERSEN. Quantum enhanced electron transfer in coupled porphyrin (Under the direction of DR. MARCUS JONES)

The role of solar power as a renewable energy source is of ever increasing importance to our future. It is inevitable then that the focus of much research would be looking at nature's solutions to solar power with photosynthesis. A theoretical paper published by Creatore et al. titled "Efficient Biologically Inspired Photocell Enhanced by Delocalized Quantum States" looks at a way around the problems that plague attempts to reproduce what biological systems do so well. Their design however tried to achieve this by exploiting transition dipole coupling between two donor molecules and an acceptor, based on well understood phenomena, instead of difficult to reproduce coherences. This should theoretically result in an approximately 35% increase in photocurrent as compared to the same systems without coupling.

The focus of this research was to create a novel cofacial porphyrin dimer system to function as the donor pair in the Creatore et al. model. A side-bridge of aliphatic carbons linking two porphyrin molecules together was synthesized. It was expected that with zinc centers in these porphyrins, addition of bipyridine would create a rigid cofacial system. The tests with nonside-bridged and bipyridine showed expected behavior for a cofacial system. The side-bridged samples however did not show any sign of the expected coupling, instead showing signs of aggregation of the porphyrin samples with the addition of bipyridine. Further exploration into the dyad made of different lengths and the obtainment of crystal structures are required.

DEDICATION

For Alisha, for always having faith in me every step of the way

ACKNOWLEDGEMENTS

During my time here at UNC Charlotte there have been numerous people who have assisted me in my goals both in teaching and in my research. My wonderful girlfriend Alisha has been with me through all the difficulties, constantly reassuring me with her constant faith. Even though she had to put up with all my stress and frustrations, she dealt with all of that with grace and made me feel good about the word I was doing when I would doubt myself.

Dr. Marcus Jones deserves a great amount of thanks from me. He was my advisor for research both as an undergraduate and as a graduate student. I have learned much from his vast physical chemistry knowledge. Thank you to Dr. Walter, who was also always available to lend his knowledge on porphyrins and organic chemistry whenever I needed it. Thank you to the rest of my Committee, Dr. Schmedake and Dr. Her. An additional thank you must be given to Dr. Stokes who substituted for Dr. Her at the last minute

Many thanks to the rest of the Dr. Jones research group: Drew, Danielle, Gaurav, Jose, and Keri. You all helped me so much with my research, either with direct assistance or as someone off which to bounce ideas. I also would not have been able to successfully complete the synthesis of this project without assistance from Dr. Vivero-Escoto and Daniel Vega. Monica Rabinovich was an excellent guide for my time as a TA and had confidence in me even when things were not going well in my labs. Lastly I would like to thank Robin and Caroline for helping me with paperwork, scheduling and printing, making sure I stayed on schedule.

There are so many people who helped me in my time here at UNC Charlotte and I surely wouldn't have gotten through this program without the assistance they provided. I am eternally grateful to you all.

TABLE OF CONTENTS

LIST OF ABBREVIATIONS

Bpy	4,4’-bipyridine
DCC	Dicylclohexylcarbodiimide
DCM	Dichloromethane
DMAP	4-dimethylaminopyridine
DMSO	Dimethylsulfoxide
EDC	1-Ethyl-3-(3-dimethylaminopropyl)carbodiimide
LHCII	Light Harvesting Center II
NHS	N-hydroxysuccinimide
PL	Photoluminescence
PPC	Pigment protein complexs
PSII	Photosystem II
TTP	Tetratolylporphyrine
TTPa	5-(4-Carboxyphenyl)-10,15,20-tritolylporphyrin
2DES	Two dimensional electronic spectroscopy

CHAPTER 1: INTRODUCTION

1.1 Biological Inspirations

1.1.1 Biological Photosystems

The ability to efficiently harvest light and use it for our own purposes is of ever increasing interest to scientists. Whether it be for use in generating electricity using photovoltaics, storing energy in photochemical cell or whatever other optical application that is being used, minimizing the amount of light energy that is lost without doing work is of critical importance. In photovoltaics, the upper limit of efficiency is known as the Shockley-Queisser limit, which accounts for all sources of loss for a device of a particular band gap[1] Use of organic based molecules in such devices has been a field of much research with great strides made recently in the increase of efficiency. One porphyrin based photovoltaic device recently reached a new record of 13%[2].

While our own artificial based devices are improving a very fast rate, understanding the loss of energy in these systems and finding solutions is the key goal of this research. These systems work in principal the same as systems already in existence in Nature. Nature has had to deal with the same issues before in the evolution of photosynthesis. The solutions nature has implemented has resulted in absorbed photon to conversion efficiencies near unity[3-7].

Plants and other photosynthetic life have the challenge of trying to absorb as much of the light that falls on them as possible and then using as much of the absorbed

energy as possible. To understand how plants accomplish this, the design of the plants light harvesting system must be investigated more closely. The light-harvesting photosystems made up of many protein-pigment complexes (PPCs) and a reaction center[4]. The reaction centers are where the energy is actually used to do work as part of the photosynthesis process. The PPCs act as donors, effectively enhancing the absorption cross section of the reaction centers[3]. The vast number of PPCs allow the photosystems to absorb nearly every photon that falls on them[6]. To work effectively, the photosystems have to transport the absorbed energy through a network of multiple PPCs to the reaction centers with as little loss of energy as possible[3].

Photosynthetic organisms have had to overcome several major hurdles to make this work effectively. The dense packing of the pigments within the PCCs is more than enough to lead to quenching of the chlorophyll chromophores[3]. The PPCs are designed with the spacing and orientation of the contained chromophores optimized to maximize the absorption of light by any polarization while preventing much of the quenching effects ensuring maximum capture of sunlight[3].

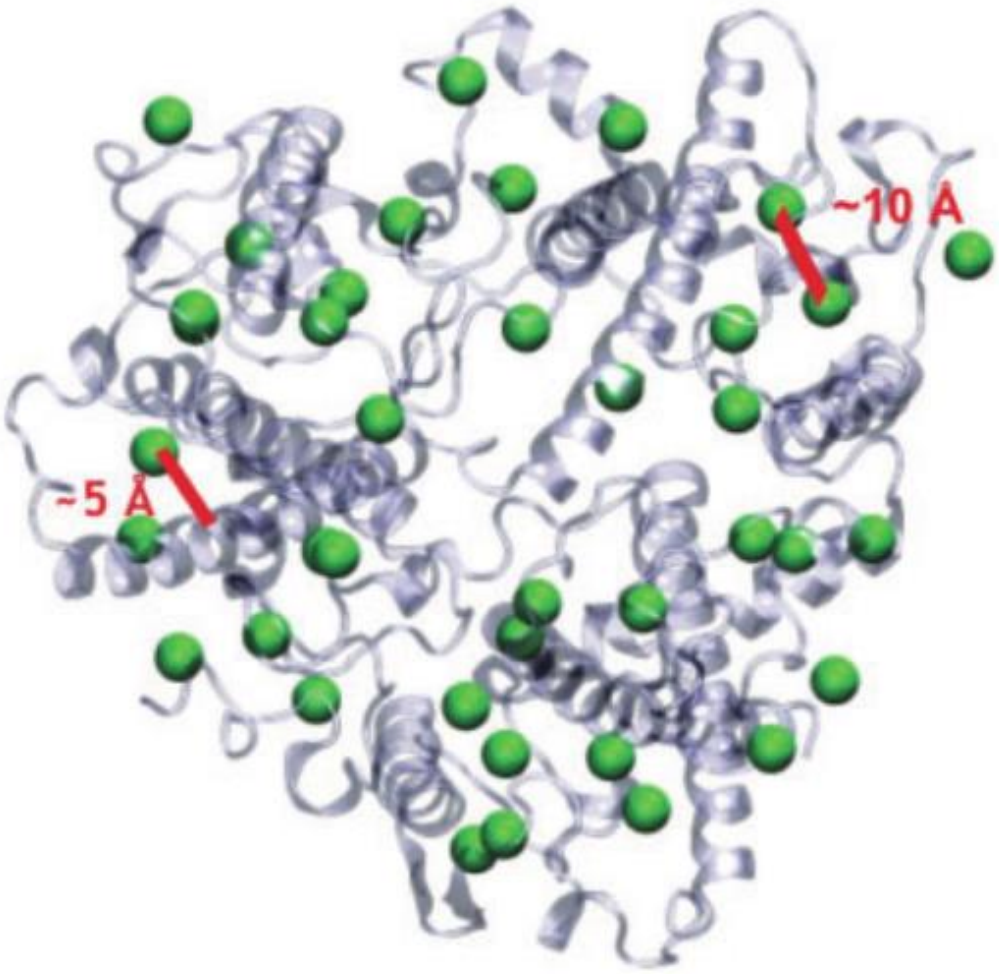

Figure 1.1[3] Structure of the PPC LHCII showing very close spacing of the chlorophyll chromophores within the protein.

Once absorbed, the PPCs are still tasked with the delivery of the energy to the reaction center without loss. In order to ensure that other photochemical processes, like emission for example, do not hemorrhage energy from the system before reaching the reaction center, the delivery of the energy to the reaction center must be very rapid, out competing the other processes[3]. To explore what rapid processes are at work, researchers

have focused on the light-harvesting center II (LHCII), the most biologically abundant PPC in the world[3] and photosystem II (PSII)[3-6].

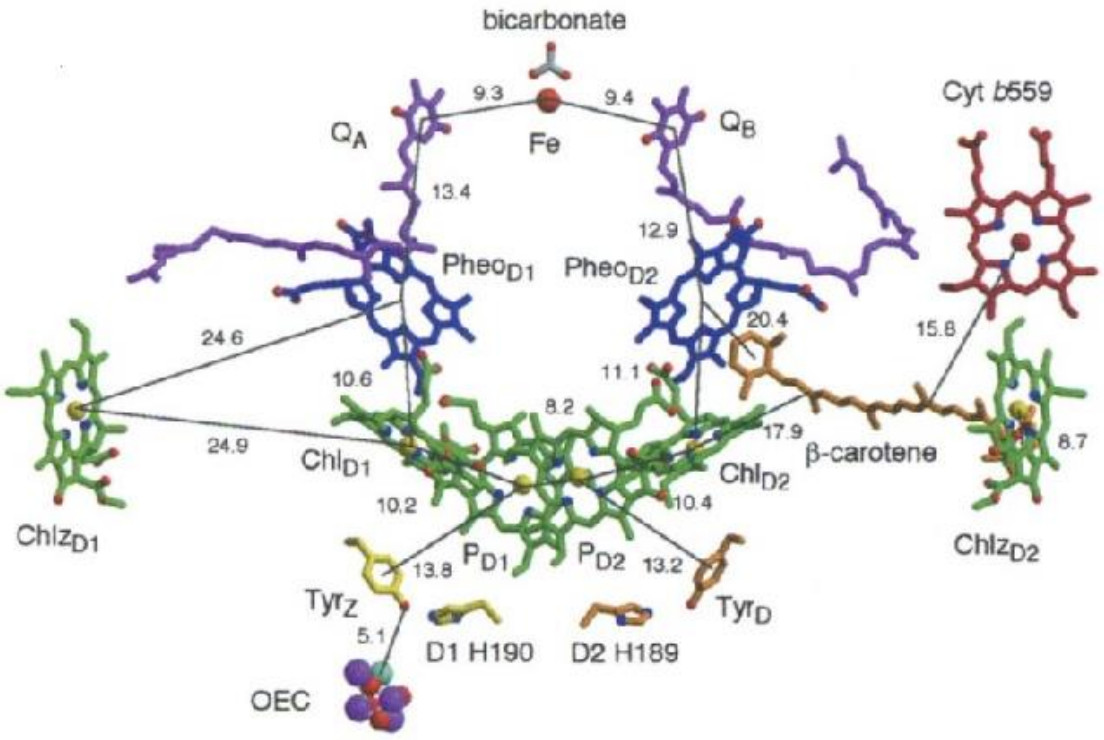

Figure 1.2[8] Structure of reaction center "special pair" and associated acceptor and other peripheral molecules. The chromophores of the pair are labeled P_{D1} and P_{D2}

1.1.2 Quantum Effects in Photosystems

Part of what allows this ultrafast transfer of energy to occur is the very dense structure of chromophores with the PPC. The light-absorbing centers are so close to one another, strong coupling can occur between them[3]. Probing the exact dynamics of these systems though proved difficult for a long time due to the incredibly short time frames involved in the process. It has been calculated that the time frame of each jump in the chain must be shorter than 300 femtoseconds for the observed quantum efficiencies[6]. Attempts to use more classical approaches to explain these rates and the overall

efficiency fell short on explaining the whole picture[3, 6]. Ultrafast femtosecond spectroscopic techniques provided the means to explore the underlying quantum processes at work and cast light on this mystery.

Using two dimensional electronic spectroscopy (2DES) has allowed the probing of these quantum effects[3-4]. 2DES is a four wave mixing process that can elucidate energy transfers between chromophores with respect to time. It has been used to show that the energy transfer between chromophores in these systems show a defined oscillation with respect to time[3-6].

1.1.3 Quantum Coherence

The oscillation seen in the energy transfer from the 2DES experiment is signature of an effect called quantum coherence[3-6] Quantum coherence is a superposition of that exists between exciton states[6]. Quantum coherence is a key part of understanding the high efficiencies of these biological photosystems[3-6]. In short, quantum coherence results from the perturbation of the system by an electromagnetic field. This causes the populations of the different states of the system to oscillate between one another. The frequency of this oscillation is given by the energy difference between the coupled states[3]. Interactions with the environment, like thermal interactions for example, cause the coherence to start to break down also called decoherence or dephasing[4]. The phase relationship of the polarization of the system and the applied field become scrambled and the coherence is lost. The time it takes for loss of coherence is known as the dephasing time. This differs from incoherent systems, where the states are not coupled, and there is no phase relationship.

Accurate measurements of these quantum coherences within biological photosystems show several interesting factors. One is that the coherences are extraordinarily long lived even at normal environmental temperatures, on the order of 700-900 fs for LHCII[4]. This timescale is longer lasting than the energy transfers within the PPC showing that coherences do last long enough to play a role in the efficiencies of the photosystems.

It seems likely that these strong and long-lived coherences are playing a direct role in the transfer of energy in the system. For a more complete understanding into why these coherences have such a strong impact on the efficiency of the systems, a look at electronic energy transfer from a quantum perspective is required. For energy transfer to happen, there must be some form of electronic interaction between a donor and acceptor. An excited molecule will transfer its energy to another if its deexcitation transition dipole couples to the excitation transition dipole of another molecule[6]. The coupling of these two molecules is highly distance dependent. The PL spectrum of the donor must also overlap with the absorption spectrum of the acceptor, to conserve energy in the system[6].

Due to the highly dense nature of the way chlorophyll is packed within the PCCs, the coupling between them is quite strong. This violates one of the assumptions Förster energy transfer that the coupling should be weak[6]. The quantum effects enter the picture in the way in the actual path the energy will follow through the system. Quantum physics allows for the exciton to follow multiple simultaneous paths through the system. The pathways can interfere either constructively or destructively. When the waves of two different paths interfere constructively, the interference can boost the energy transfer efficiency. The long lived quantum coherences in the system seem to be what allow

enough time for this to occur[5-6]. In spite of numerous observations that coherences are involved, no clear mechanism for the longevity of the coherences has been determined[9].

1.2 Mimicking Biology

1.2.1 Artificial Coherent Photosystems

Knowledge of these coherent processes in these biological systems has led many researchers to attempt to imitate the same processes in artificial systems. Dugan Hayes et al[9]. worked on exploring the possibility of long lived coherent excited states in small molecular systems. They wanted to recreate what has been already seen in biological systems. They created a series of molecules that contained two different chromophore centers held together through their molecular bonds quite rigidly. They were able to measure coherences in their systems using 2DES and found long lived coherent excited states just like for the biological systems. They concluded through their work that these long-lived coherences can arise from having a fixed close arrangement of chromophores in space that are electronically coupled[9].

Dorfman et al.[10] lead another group to explore the application using these long lived coherences. They wanted to apply the coherences to drive quantum heat engines to create more advanced artificial devices such as photovoltaics and lasers. There work used only noise based coherences instead of excitation from a more coherent source like a laser. Their designs were predicted to generate a 27% enhancement of photocurrent over systems in the absence of coherence.

1.2.2 A “Special” Special Pair

All of this recent work does show the amazing power of coherent systems, certainly they have an incredible power to efficiently drive photochemistry. They do however depend on an exact parameters to function properly which can be hard to mimic

in a laboratory setting. Creatore et al[7]. proposed a system design that tries to avoid looking at coherent processes, instead looking to dipole interactions to create quantum enhanced electron transfer through interference. The coupling of the transition dipoles is a well understood phenomena already[11-14]. The unique addition to this system is the exact way in which an acceptor can also be coupled to this donor pair. The system design is relatively simple system will be the main focus of this research, trying to recreate the propose system, then characterize it. The main premise of Creatore et al.'s design is the strong coupling through dipole-dipole interactions of two donor molecules interacting with a third molecular acceptor, seen below in Figure 3. They even noted that this is similar in appearance to the special pair in a photosystem reaction center (RC), except in the RC's case, the dipoles are not aligned.

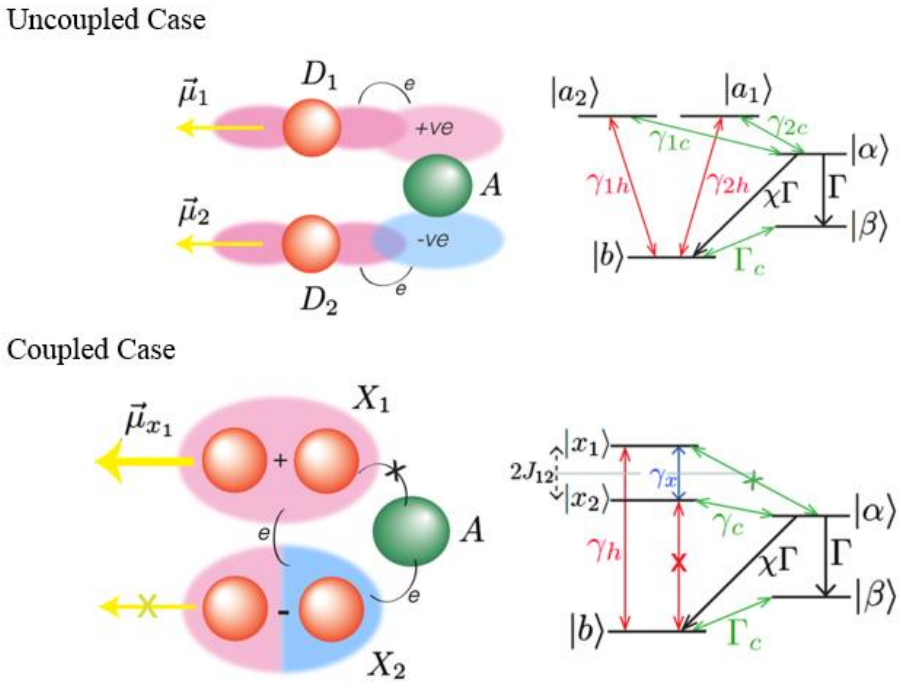

Figure 1.3[7] basic schematic of the system in a coupled (top) and uncoupled state (bottom). The coupled case creates two possible excite states a bright symmetric state at higher energies, and a dark antisymmetric at lower energies.

To explain this system, first the interaction of the two donor molecules must be discussed. The two donors, D_1 and D_2 must be arranged relative to one another such that the transition dipole moments are perfectly parallel and fixed relative to one another. This should enable strong coupling between the two donor molecules. Once coupled the excited states of the molecules are no longer degenerate and instead split into two distinct eigenstates, the symmetric $|x_1\rangle$ and the antisymmetric $|x_2\rangle$. In the absence of an acceptor, absorption happens into the $|x_1\rangle$ state and quickly relaxes into the lower energy $|x_2\rangle$ state. The $|x_2\rangle$ is antisymmetric, which means that the transistion dipoles of the two donors cancel out due to destructive interference, blocking the direct relaxation back to the ground state $|b\rangle$. Without an acceptor, the only path by which electrons in the $|x_2\rangle$ state can relax if it is thermally excited back into the $|x_1\rangle$ state which then relaxes back into the ground state[7].

That is the picture for the two donors, the acceptor is crucially just as important as the donors as is its positioning in the system. The two donor molecules must also be coupled to the acceptor such that the two states $|x_1\rangle$ and $|x_2\rangle$ can interact either constructively or destructively with the acceptor. In the symmetric case of the donors, there is destructive interference with the acceptor. Since both of the donors are in the same phase, there is going to be a destructive overlap between one of the donors and the acceptor. This means that the transition from $|x_1\rangle$ into the acceptor state $|\alpha\rangle$ is forbidden. The transition from $|x_2\rangle$ to $|\alpha\rangle$ though is subject two constructive interference for the same reasons. This means that the system is set up in such a way as leave the electrons with few options but to go through the system as a quantum heat engine. There are some losses though due to relaxation from $|x_1\rangle$ back down to the ground state instead

of $|x_2\rangle$. There is also loss from thermal repopulation of $|x_1\rangle$ from $|x_2\rangle$ followed by relaxation to the ground state. The overall effect though is still considerable from the uncoupled system, showing a 35% enhancement of photocurrents from the device using reasonable conditions in the calculations[7].

1.2.3 Pauli Master Equations

The mathematical basis for this system design lies in the Pauli master equations (PME). These equations for the following system are:

Equation 1[7]

$$\dot{\rho}_{x_1x_1} = -\gamma_x\left[(1+n_x)\rho_{x_1x_1} - n_x\rho_{x_2x_2}\right] - \gamma_h\left[(1+n_h)\rho_{x_1x_1} - n_h\rho_{bb}\right]$$

$$\dot{\rho}_{x_2x_2} = \gamma_x\left[(1+n_x)\rho_{x_1x_1} - n_x\rho_{x_2x_2}\right] - \gamma_c\left[(1+n_{2c})\rho_{x_2x_2} - n_{2c}\rho_{\alpha\alpha}\right]$$

$$\dot{\rho}_{\alpha\alpha} = \gamma_c\left[(1+n_{2c})\rho_{x_2x_2} - n_{2c}\rho_{\alpha\alpha}\right] - (\Gamma + \chi\Gamma)\rho_{\alpha\alpha}$$

$$\dot{\rho}_{\beta\beta} = \Gamma\rho_{\alpha\alpha} - \Gamma_c\left[(1+N_c)\rho_{\alpha\alpha} - N_c\rho_{\beta\beta}\right]$$

$$\rho_{x_1x_1} + \rho_{x_2x_2} + \rho_{\alpha\alpha} + \rho_{\beta\beta} + \rho_{bb} = 1$$

Solving these equations for the coupled case and comparing it to similar solutions for the uncoupled case, Creatore et al were able to create equations of the populations of different states with respect to time, (figure 1.4).

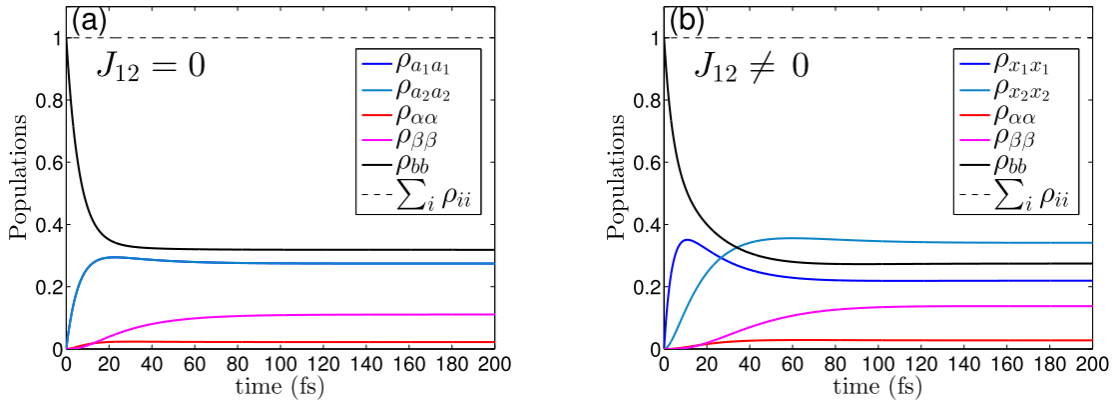

Figure 1.4[7] Graphical solutions to the Pauli master equations showing populations of different states with respect to time from beginning of excitation for (a) uncoupled and (b) coupled donors.

The solutions for the uncoupled case there is no difference between the populations in the excited states of either donor, $\rho_{a_1a_1}$ and $\rho_{a_2a_2}$, caused by their degeneracy. A significant difference can be seen in the solutions for the coupled system. The now non-degenerate donor excited states are no longer overlapping due to the new energy levels and transitions rules. Following excitation, the population of the $|x_1\rangle$ state begins to rise first but it quickly peaks and begins to decrease as its population begins to relax into the $|x_2\rangle$ state which itself cannot be directly excited, this causes the $|x_2\rangle$ population to start to grow. For both cases now, transfer between the excited donor states and the excited acceptor state, $|\alpha\rangle$, occur. Though it is difficult to tell from the graph, the couple situation results in a higher population in the $|\alpha\rangle$ state, a manifestation of the quantum enhancement effect.

1.2.4 Effects of Dipole Angle

The group conducted a detailed study onto the effects of different parameters such as dipole angles between the donors, phonon rates and temperature. Calculations were performed for each of these variables to measure their effects on the system. The first

thing to look at is the effect of dipole angles on the system[7]. A graph of the effect of the angle between the dipoles of the donors on the quantum enhancement effects can be seen below in figure 5.

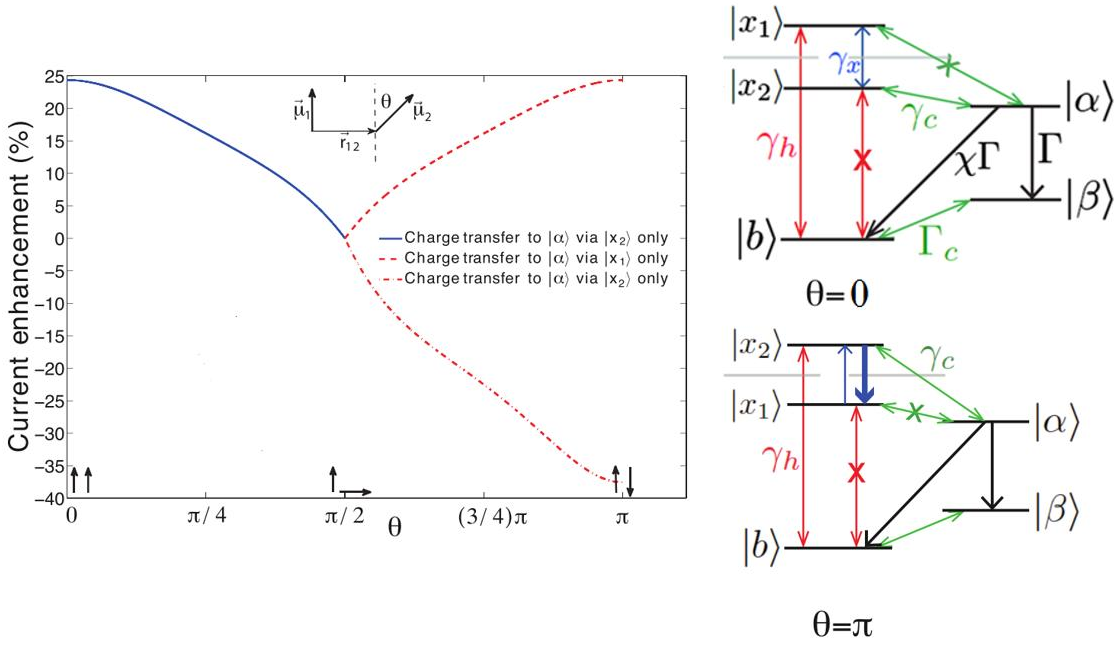

Figure 1.5[7]. The graph on the left shows the effect of angle on current enhancement of the system. The blue line represents the angular effects between 0° and 90°. The red dashed lines cover the regimes for angles greater than 90°. The two different lines refer to enhancement from the two different donor excited states. The right shows energy schematics for angles of 0° and 180°

For maximum coupling between the donors, the dipoles must be aligned exactly parallel or 0 degrees. As the angle between the dipole moments starts to grow, the coupling becomes weaker and the splitting caused by the coupling becomes less, until the angle reaches 90 degrees, at this point there is no coupling between the system and the excited states are degenerate. It is as the angle passes 90 degrees that the system starts to behave a more different than has already been discussed. Taking it all the way to the completely antiparallel arrangement makes this differences easier to discuss. The two couple excited states reverse places with the symmetric $|x_1\rangle$ state becoming the lower

energy dark state, and the antisymmetric $|x_2\rangle$ becoming the higher energy bright state. New transition rules now apply too as $|x_1\rangle$ to ground state is now forbidden, $|x_2\rangle$ to ground state is now allowed, and the transition from donor to acceptor is now only allowed from the higher energy bright state. This antiparallel arrangement significantly inhibits the quantum enhancement of the system. This can be seen from the huge negative effect on the photocurrent from the $|x_2\rangle$ state. It is therefore crucial to have the system as rigidly locked into the parallel dipole arrangement as possible[7].

1.2.5 Effects of Transition Rates

Another important aspect of this system is how the transitions rates. Specifically between the $|x_1\rangle$ to the $|x_2\rangle$ states and from $|x_2\rangle$ state to the acceptor effect the enhancement of the photocurrent, notated as γ_x and γ_c ($\gamma_c = \gamma_{1c} + \gamma_{2c}$) respectively. This analysis however only shows the relative enhancement of photocurrents compared to the rates for the uncoupled case.

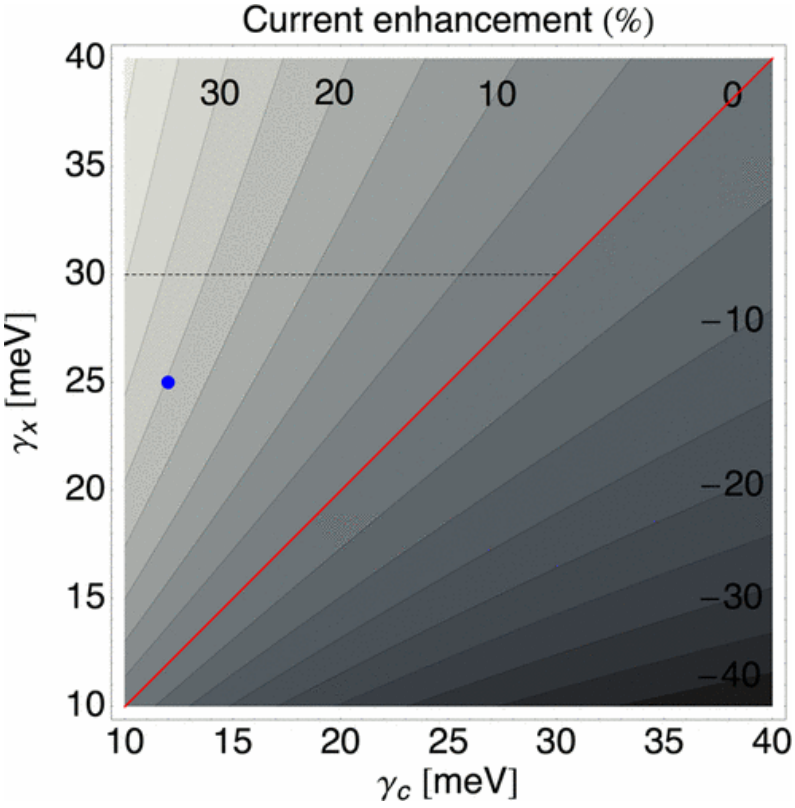

Figure 1.6[7]. Contour map of the relative current enhancement for various rates of γ_x and γ_c. The blue dot represents a set of rates used in most calculations ($\gamma_x = 25$ meV and $\gamma_c = 12$ meV) with an enhancement of 25 percent. The dotted black line is the upper limit of γ_x where $\gamma_x = 2J_{12}$. Black line is for when the rates are equal, showing zero enhancement.

As figure 1.6 shows, the relative enhancement is the highest when $\gamma_x > \gamma_c$ when compared with the case of no coupling. Looking at γ_x, for higher values of this rate, it means faster transfer of electrons from the $|x_1\rangle$ to the $|x_2\rangle$ state. The faster electrons transfer from the bright $|x_1\rangle$ state to the dark $|x_2\rangle$ state, the fewer electrons can relax back down to the groundstate, so the transition from the $|x_1\rangle$ to the $|x_2\rangle$ can better outcompete the emissive relaxation of the bright state. In the dark $|x_2\rangle$ state now, the electrons are effectively trapped with only one outlet, the transfer to the acceptor, forcing the system into doing more work. When $\gamma_x = \gamma_c$ there is no current enhancement since $\gamma_x = \gamma_c = \gamma_{1c} + \gamma_{2c}$. This means that the rate through the path created by the coupling, $|x_1\rangle$ to $|x_2\rangle$ to $|\alpha\rangle$, is the same as the combined rates of the uncoupled system, $|a_1\rangle$ to $|a_2\rangle$ to $|\alpha\rangle$. When $\gamma_x <$

γ_c the rate is not competitive with the uncoupled system, and negative enhancement is seen. To increase relative enhancement then, one can either increase γ_x or decrease γ_c. There are limitations to this, γ_x can only be as large as $2J_{12}$, creating an upper limit. Decreasing γ_c will also create a higher relative enhancement compared to the uncoupled system, however this lowers the absolute current of the system as electrons are not efficiently transferred from donor to acceptor and simply build up in the $|x_2\rangle$ state[7].

1.2.6 Effects of Temperature

Lastly, we can look at the effects of temperature to the system. As temperature decreases in the system, the population of thermal phonons will be lower. At room temperature, the normal population of phonons can interact with electrons in the $|x_2\rangle$ state, allowing for the energetically uphill transition into the $|x_1\rangle$ state. At lower temperatures there is a lower population of phonons, and the uphill transition happens less often. This is an interesting situation as normally photoluminescence of the system would drop as temperature was increased, this system however would be more emissive at higher temperatures and less emissive at lower temperatures. This quirk of the system is useful though as it means less energy is being lost through thermal repopulation and emission from the bright state, increasing the current enhancement effects[7].

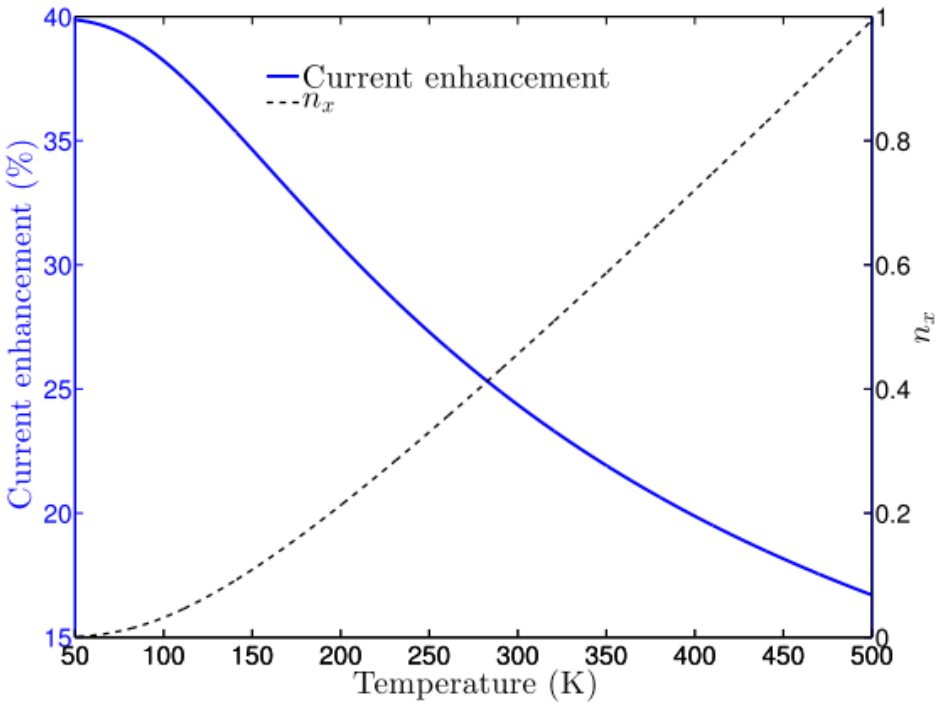

Figure 1.7[7]. The dependence on temperature of both current enhancement % (blue) and the phonon population (dashed black).

1.3 Designing a Real World System

1.3.1 Prophyrins Provide the Solution

The system designed by Creatore et al[7]. is ingenious and based on simple well understood mechanics. What their paper lacks, however, is an actual real world example of the theoretical system. The task now at hand is to design a molecular system such that it can obey the criteria defined by their calculations. Taking a lesson from the "biologically inspired" aspect of this system, porphyrins were turned to as a solution. They are strong absorbers in the visible region of the light spectrum, and their structure and an appropriate metal center allows for easy co-facial dimerization leading to a donor pair that can be held in fixed positions to one another. That still leaves the issue of

aligning the dipole moments of the two porphyrin and attaching it to an acceptor in the correct orientation. While co-facial porphyrin dimers are fixed in terms of distance orientation of the rings, always being parallel, they are however free to rotate around the linker bonds that connect them. This is a problem for controlling the relative angle of the two dipoles. The acceptor also presents a problem as it must be aligned in a particular way to the donors in order to function.

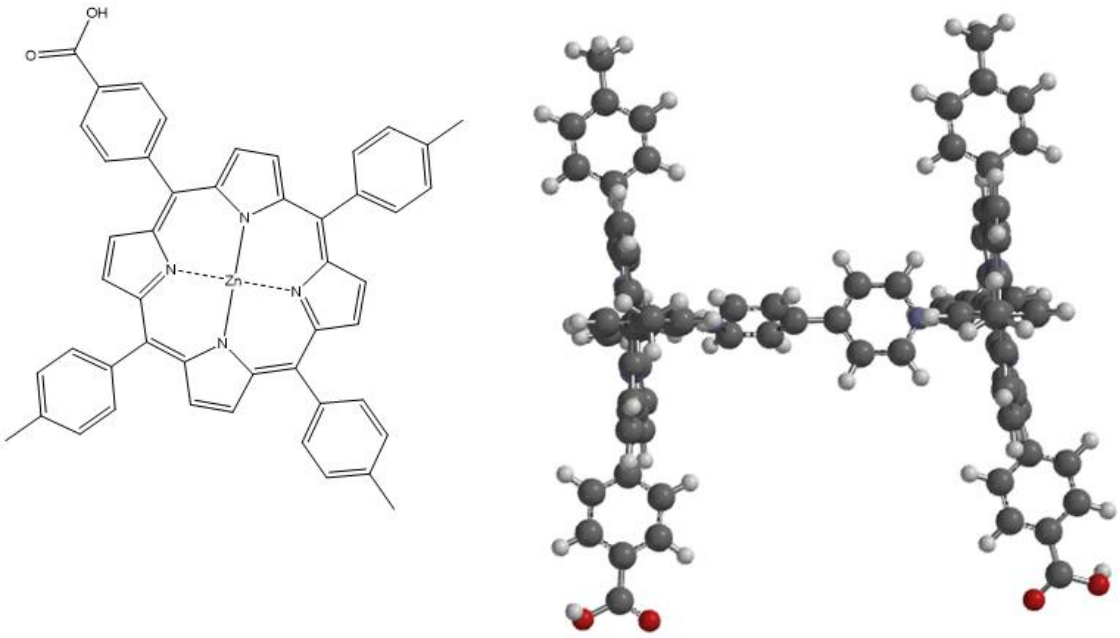

Figure 1.8: The left is the asymmetric zinc TTPa structure. The right is the proposed dimer system, linked by 4,4'-bipyridine in the absence of an acceptor. This arrange though still allows for free rotation about the metal center, therefore parallel transition dipoles is not likely.

Our solution to these remaining problems was to use an asymmetric porphyrin. Specifically one that seemed quite promising is 5-(4-Carboxyphenyl)-10,15,20-tritolylporphyrin (TTPa)[15], the structure of which can be seen below in figure 8. The lone carboxylate group on one side provides the place where we can attach the acceptor. The acceptor would be appropriately positioned, assuming correct orientation of the orbitals,

and would also prevent rotation of the donors. The metal center chosen was zinc as it will only coordinate on one side of the porphyrin ring. This means that only dimers will be formed and not any long chains of porphyrin molecules. 4,4'-bipyridine was chosen as a potential linker for early experiments due to rigidity and linear spacial relationship of the two coordinating nitrogen atoms. Additionally, 4,4'-bipyridine has an additional quality of not absorbing visible like or interacting with the excited stated in zinc porphyrins[16-18]. This allows for the creation of a system that should keep the planes of both porphyrins parallel and there distance to remain constant. Lastly, pyridine ring moieties coordinate well with zinc metallated porphyrins for use of cofacial dimer creation or the attachment of other molecules[19-22]

1.3.1.1 Creating the Donor System

It is the primary focus of this research to make and characterize the coupled donor pair to which an acceptor can later be added. The binding of the bipyridine is not enough in this case do to free rotation of the porphyrin rings preventing optimal transition dipole alignment. In the completed system the acceptor will also serve to prevent rotation, this rigidity must be mimicked without the use of an acceptor or significantly altering the properties of the system. To solve the problem of rotation, a side bridge of aliphatic carbons was added to the design of the system. Carbon chains are ideal as the length can be varied as needed to suit the system with different crosslinking ligands.

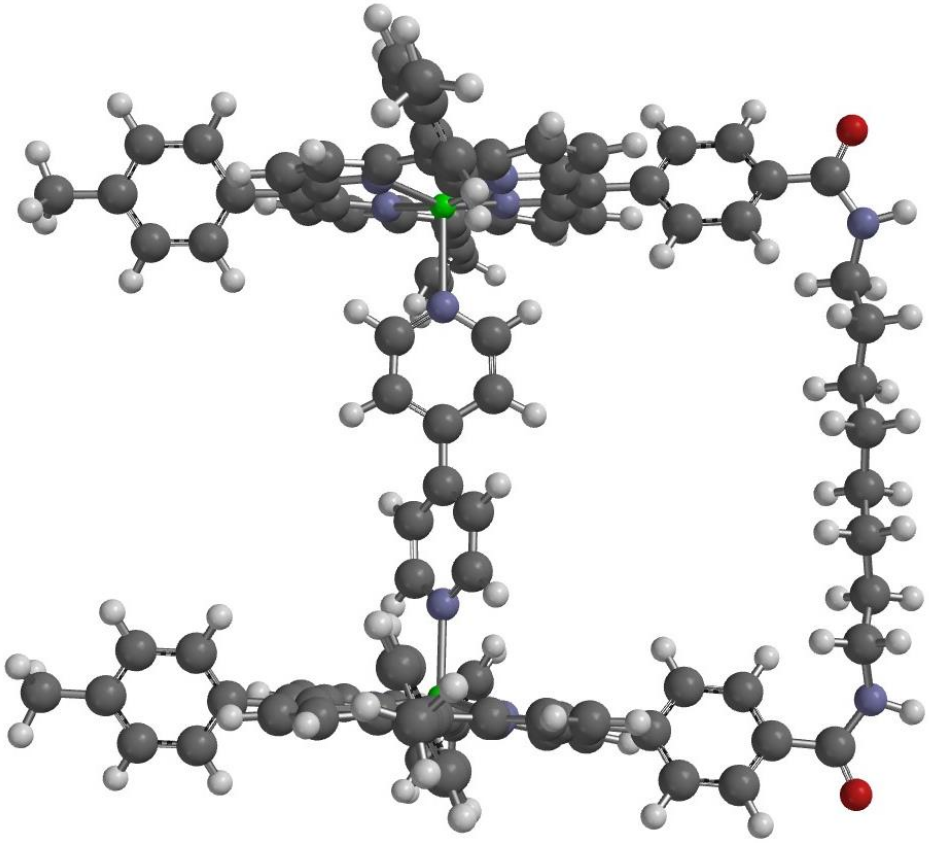

Figure 1.9: Cofacial porphyrin with added side bridge to prevent free rotation.

1.3.2 Past Research on Cofacial Porphyrin Dimers

In the past, much work has been conducted on co-facial porphyrin dimers, while the approach taken in thesis is novel in some respects, previous system can be looked to for great deals of information on the subject.

Crown ether moieties have been used for dimerization. Porphyrins substituted with form crown either groups around the ring will dimerize upon the addition of the appropriate metal ion for the crown ether to chelate. D'Souza et al.[23-24] designed a porphyrin dimer system similar to the one proposed with two zinc porphyrins linked cofacially coupled with a fullerene acceptor to mimic the RC special pair. Upon the

addition of potassium ions, the crown ethers would chelate the ions and form the dimers. Their system had the transition dipoles of the two porphyrins nearly parallel, varying by a few degrees, and their fullerene acceptor was not oriented the same way with respect to the donors. Nikolaitchik et al. used a similar method employing pthalocyanines instead of porphyrins[25].

Other methods of dimerization utilize covalent bond and steric hindrance to ensure the porphyrins are cofacial. One approach is to diarylurea bonds on the ortho or meta position of an aryl ring attached to the meso position of the porphyrin[26-28]. This approach is prevented from rotation by the steric interaction of the rings, and can be increased with additional substitutions on the aryl ring[27]. As such, systems with a side bridge formed from just one of the four meso positions on the porphyrin is enough to ensure cofaciality. In addition to the diacylureas, fused rings and ether moieties can be used to form dimers as well[29-32]. Some of these systems might not have quite the right geometry or are too rigid for perfect cofaciality[30].

Cofacial porphyrins can also be formed by coordination off the metal center. 4,4'-bipyridine and other similar ligands can be used to bridge the metal center of two or more porphyrins[33-41]. Certain metals like zinc can only coordinate from one side when part of a porphyrin molecule, so that these crosslinking ligands form dimers. Other metals that bind on both sides can be used to construct long chains of cofacial porphyrins. Bipyridine has been shown by these papers to bind well with zinc metalloporphyrins[36]

1.4 Background on Porphyrins

1.4.1 Introduction to Porphyrins

Porphyrins are a class of molecules of great importance to biology ranging from the heme porphyrin found in hemoglobin, to the major pigments of plants, chlorophyll. Prophyrins are ubiquitous to biology, filling roles in oxygen binding and transport, electron transfer, catalysis, and light harvesting during photosynthesis[42-43]. These molecules consist of a backbone of four pyrrole rings linked together in a larger cycle by four methine bridges. The extended aromatic conjugation of the system allows for strong absorption bands in the visible light spectrum and therefore have a good spectral overlap with incident solar radiation[42].

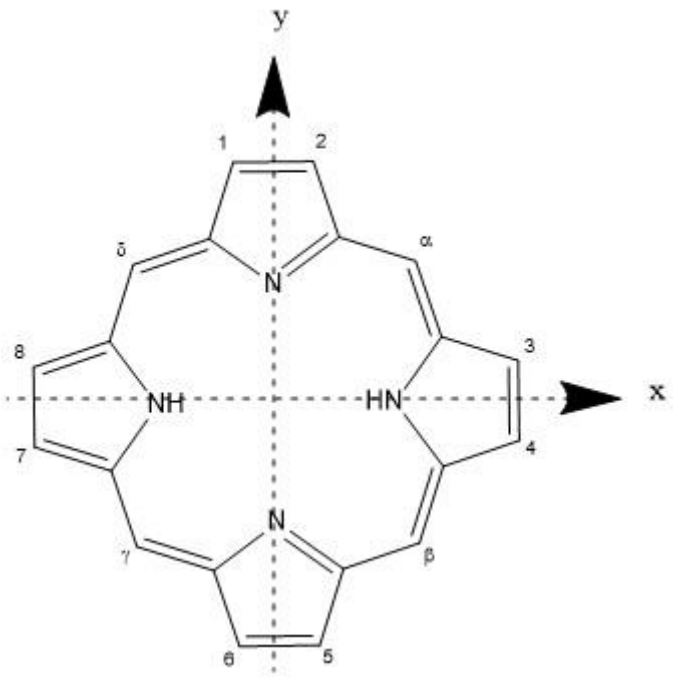

Figure 1.10. Basic porphyrin skeleton with the positions where modifications to porphyrins can be attached, Greek letters denoting the meso positions and transition dipole arrows shown.

1.4.1.1 Metalloporphyrins

The arrangement and spacing of the four nitrogen atoms in the porphyrin ring are ideal for forming tetracoordinate complexes with many metal ions forming a metalloporphyrin. For smaller metal ions, they can fit perfectly into the ring plane of the porphyrin forming a regular metalloporphyrin. Some metal ions such as zinc still have an available coordination site while within the porphyrin ring, allowing an additional ligand to attach to form an overall geometry of square pyramidal for the metal center. Other metals can bind on bother sides of the porphyrins for an octahedral geometry. However for larger metal ions, the porphyrin can still chelate the ion, but the metal is incapable of fitting completely within the porphyrin ring, instead sticking out to one side of the ring plane forming the sitting-atop (SAT) metalloporphyrins

1.4.2 Spectra of Porphyrins

1.4.2.1 Absorption Spectra of Porphyrins

As mentioned previously, porphyrins have strong absorption in the visible spectrum arising from the aromatic conjugation. These absorption bands can be divided into two different groups, the Soret bands, sometimes referred to as B-bands and the Q bands. The most intense of these absorptions is the Soret bands, with typical peaks occurring around 400 nm, with molar absorptivities of 10^5 M^{-1} cm^{-1} [42-45]. The Q-bands while also fairly intense for absorptions, are far weaker compared to the soret bands with molar absorptivities in the 10^3 M^{-1} cm^{-1}. Q-bands absorption occurs in the 500-750 nm range[42-45]. In free base porphyrins, the Soret-bands are typically show up as one tall peak with high energy shoulders and the Q-bands consist of four distinguishable peaks.

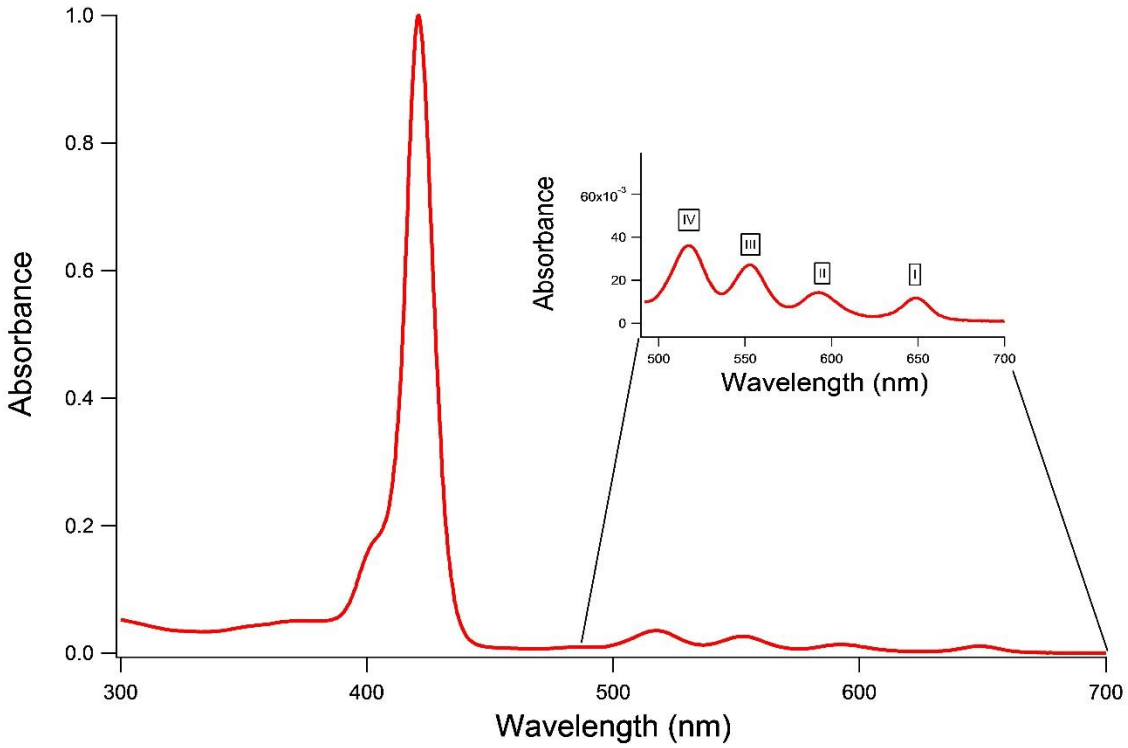

Figure 1.11: typical absorption spectrum of a free base porphyrin with inset enlargement of the Q-Bands

Porphyrins exist in many modified forms created by functional groups attached to the porphyrin ring, reduction of double bonds in the ring, and addition of metal centers. All of these modifications can change the spectra of porphyrins and as such porphyrins are typically grouped into five different classes based on the changes to their absorption spectra. In particular these classes can be distinguished from one another based on the relative intensity of their Q-bands. These five classes are Etio, Rhodo, Phyllo, Chlorin, and Rhodin. The porphyrin TTPa to be used in this research falls into the Etio class, which can be recognized by the relative intensities of the Q bands IV>III>II>I. For other classes the relative intensities will follow a different order.

Metallation alters the absorption spectrum of the porphyrin. Depending on the exact nature of the particular metal ion and how it binds to the porphyrin, this alteration can be different. Whether or not the metal is closed shell, paramagnetic or diamagnetic,

and if it forms regular or SAT porphyrins can have a great effect on the spectrum of the porphyrin. Zinc, the metal center of interest in this research causes a simplification of the Q-bands structure, reducing the number of Q-Bands from four to two with a distinct redshift.

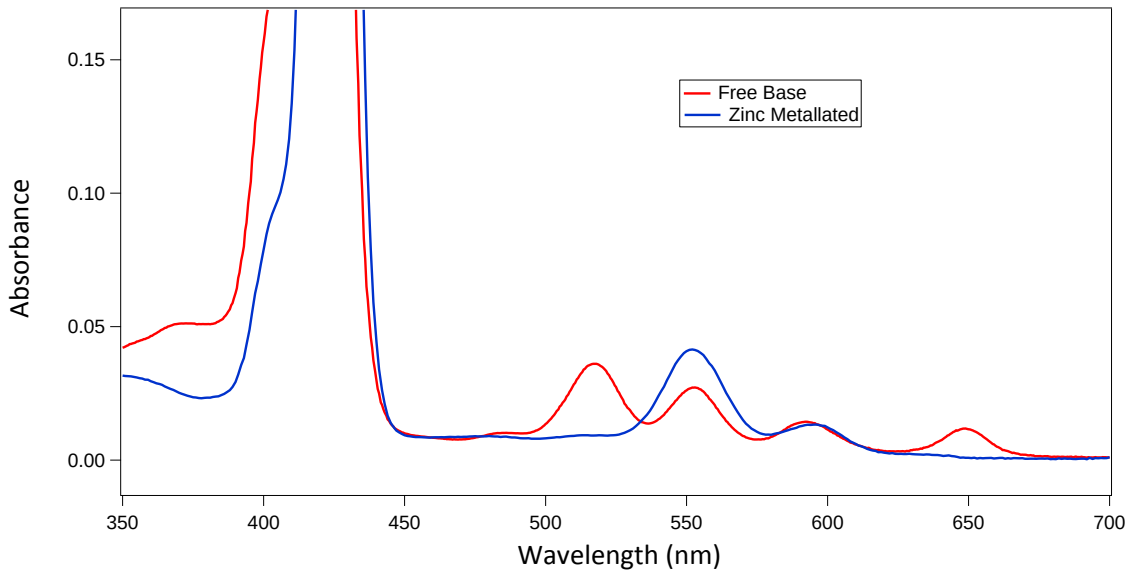

Figure 1.12: absorption spectra for free base and zinc metallated TTPa porphyrin showing a distinct redshift and Q-band reduction upon metalation.

1.4.2.2 Photoluminescent Spectra of Porphyrins

While porphyrins have quite complex absorption spectrum, their emission spectra are much simpler. Light absorbed into the soret band will undergo rapid internal conversion to the lower energy Q-bands, therefore fluorescent emission is only seen from the Q-bands. The resulting fluorescent spectrum has only two peaks. The fluorescence spectrum blue shifts upon metallation. Additionally the relative intensities of the two peaks can change. This can be seen in Figure 1.13 which shows the emission spectra for free-base and zinc metallated TTPa. Phosphorescent emission is also possible, generally seen at lower wavelengths than the fluorescent emission.

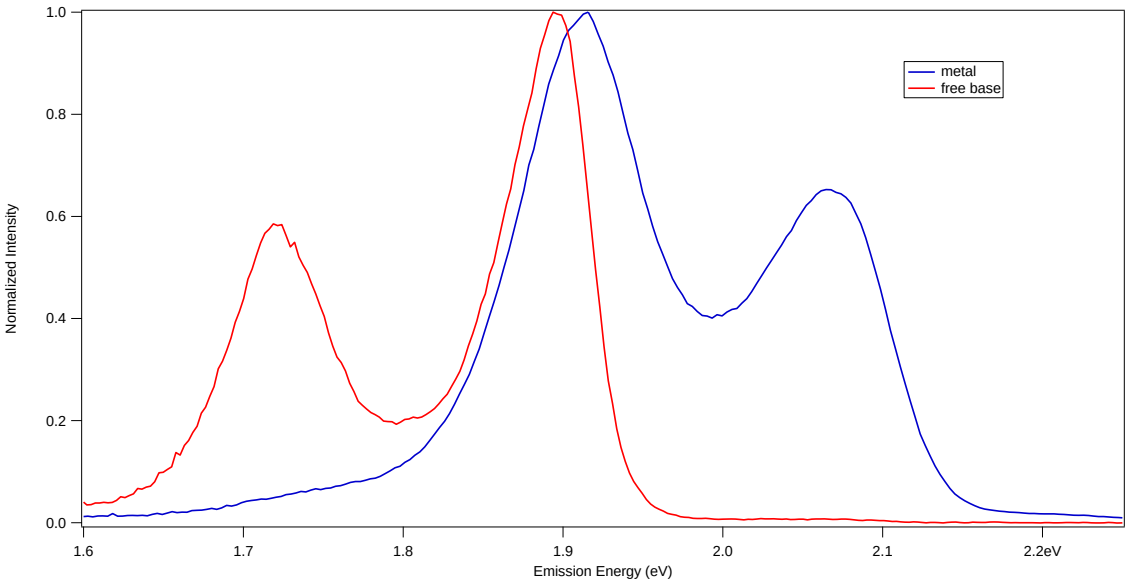

Figure 1.13: Emission spectra for free base and zinc metallated porphyrin

1.4.3 Gouterman's Four Orbital Model

In the 1960's Martin Gouterman at the Harvard University developed a "four-orbital" model for explaining the complex absorption spectra of porphyrins and their derivatives. This model is still considered to be highly accurate at describing the behavior of porphyrins today. The model is based on the idea that the majority of the optical properties in porphyrin rings are dominated by two HOMOs and two LUMO orbitals. The HOMOs are reported as being an $a1_u$ and an $a2_u$ symmetry. The LUMOs were calculated as a set of degenerate e_g orbitals. Orbital mixing splits the two excited states in energy creating two different excited states. A higher energy state with significantly greater oscillator strength corresponding to the soret peak in the absorption spectrum and a lower energy strength with lower oscillator strength giving rise to the Q bands.

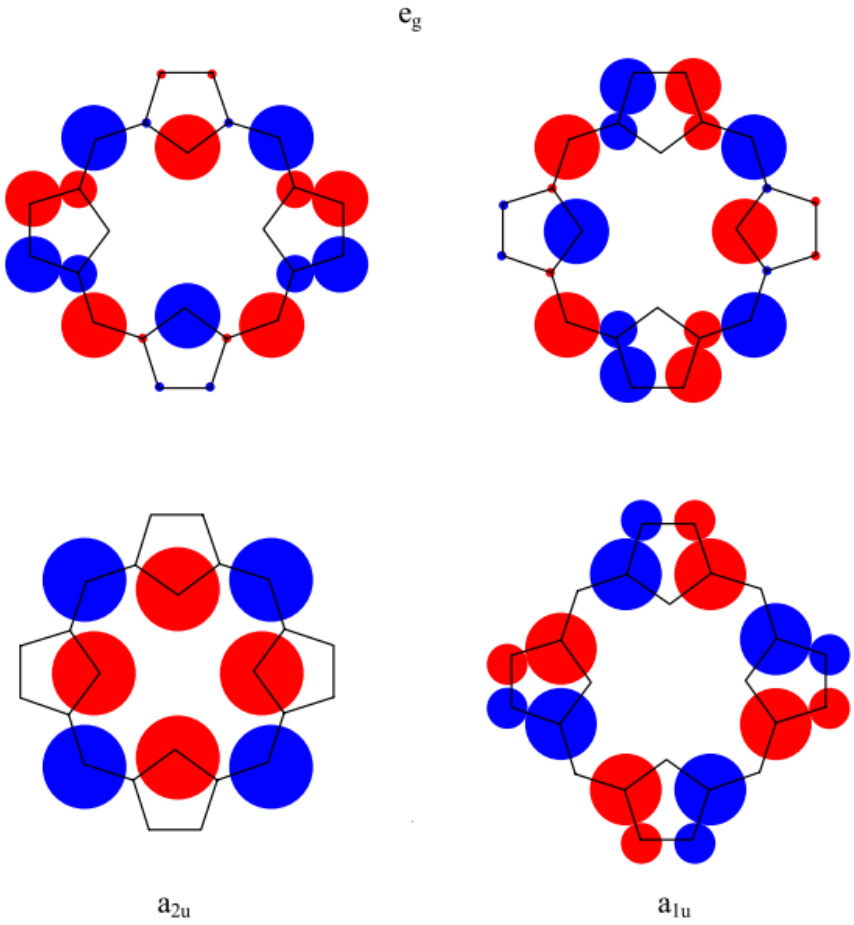

Figure 1.14[46]: The four orbitals that give rise to the spectral properties of porphyrins from the four orbital model. The two HOMO orbitals are on the bottom, the two degenerate LUMOs are on the top.

Metalloporphyrins have simpler in spectra due to the increased symmetry of porphyrin molecule when the metal center is added. Protonation of the porphyrin ring also increases symmetry and results in a similar simplification of the spectra. The shift corresponds of a symmetry of D2h for free base porphyrin changing to D4h symmetry for the metallated and protonated porphyrins.

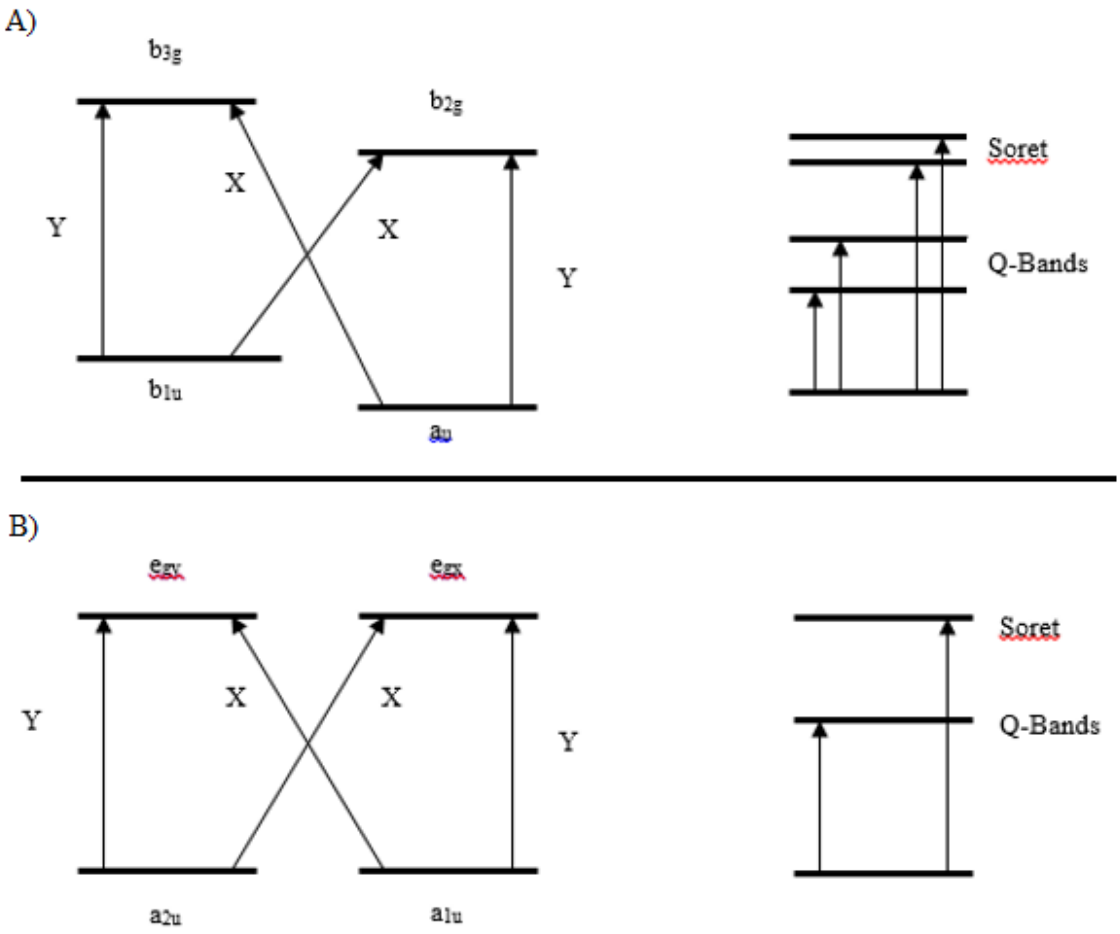

Figure 1.15[47]: Four orbital model energy diagrams for A) free base porphin and B) metallated porphin. The gain in symmetry upon metallation can be seen in the simplification MO diagrams.

CHAPTER 2: EXPERIMENTAL

2.1 Porphyrin Chemistry

2.1.1 Synthesis of TTPa

Three molar equivalents of p-tolylaldehyde and one molar equivalent p-carboxybenzaldehyde were dissolved in propionic acid. The mixture was heated to 140 °C and 4 molar equivalents of pyrrole were added dropwise over 30 min. The mixture was heated for an additional 30 min before allowing to cool. Filtering the reaction mixture yielded purple crystals[48-49].

2.1.2 Purification of TTPa

From the reaction above, six different porphyrin products are statistically possible. In addition to the desired TTPa, a tetra-tolyl substituted porphyrin, two different dicarboxylate substituted, a tricarboxylate and a tetracarboxylate product is also produced. The reaction mixture must be separated by column chromatography. A suspension of 120-230 mesh silica gel in chloroform was prepared and allowed to settle for several hours in a column. The crude porphyrin mixture was loaded onto the column. After loading, the column was run using a mixture of 1% methanol in chloroform, and a small amount of triethylamine to remove any acid in the chloroform. The first porphyrin band to elute is the least polar tetra-tolyl substituted porphyrin. The second porphyrin band to elute is the desired TTPa compound. The other higher carboxylate substituted porphyrins are more polar and are retained on the column and will not elute quickly. As

these porphyrins were not desired, the column elution was halted after the TTPa had eluted.

2.1.3 Metallation of Porphyrins

For this experiment the desired metal center for TTPa and any porphyrin derivatives is zinc. Metallation was achieved by adding an excess of zinc acetate to a solution of porphyrin in chloroform and refluxing for 1-2 h. When finished the sample is allowed to cool completely to room temperature before removing left over zinc acetate by gravity filtration. To confirm metallation, the samples were checked with UV-vis absorbance spectroscopy.

2.1.4 Synthesis of the Aliphatic Side Bridge

Several different synthesis methods were conducted in the attempt to synthesis a side-bridged porphyrin dimer of TTPa. The first type of side-bridge that was attempted to be synthesized consisted of an ester bond between the porphyrin and the carbon chain side-bridge. Three different reactions were tried to synthesize the ester bond,

2.1.4.1 Acyl Chloride Esterification

The first method used was to first synthesize the acyl chloride derivative of the porphyrin and react it with an aliphatic diol of the desired length. First, the TTPa was refluxed in neat thionyl chloride overnight to convert the acid into the acyl chloride. The thionyl chloride was removed by distillation. Neat pyridine was then added to neutralize any remaining hydrochloric acid and thionyl chloride and dissolve the acyl chloride porphyrin. To this solution, a stoichiometric amount of the diol was added to complete the synthesis. The crude reaction products were then purified by column chromatography using silica gel and chloroform.

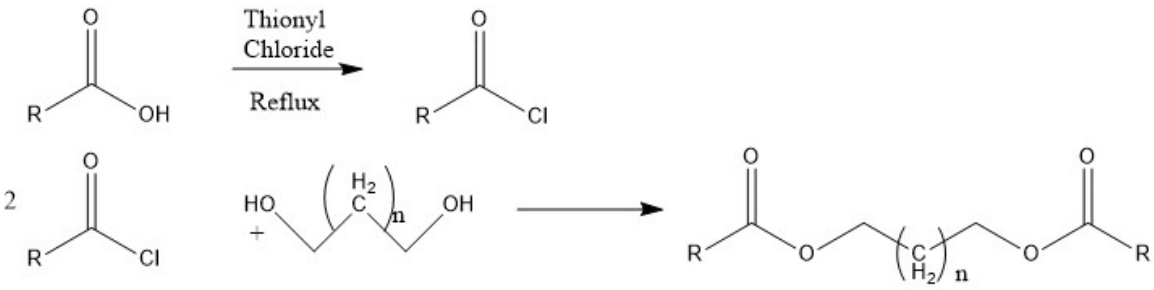

Figure 2.1: Esterification via Acyl Chloride Reaction

2.1.4.2 Steglich Esterification

Another method to try and synthesize the ester based side bridge was the use dicyclohexylcarbodiimide (DCC) which is normally a peptide coupling agent. DCC and other carbodiimides react with carboxylic acids to create a very reactive and unstable intermediate which can act as a leaving group for the reaction. While this method tends to work well for making amides as the reaction between the amine and the DCC-acid intermediate is much faster than the lifetime for the intermediate. For esters however, the reaction is much slower and the intermediate breaks down too fast for ester formation to occur. To solve this, 4-dimethylaminopyridine (DMAP) is used to react with the DCC intermediate to make a more stable intermediate, giving the alcohol groups time to attack and make the ester bond. The reaction for the side bridge was carried out with by mixing the porphyrin and diol with DCC and DMAP with the diol as the limiting reactant to ensure formation of the dimer, and not a monoester porphyrin. The products were purified by column chromatography using silica gel and chloroform.

Figure 2.2: Steglich Esterification Reaction

2.1.4.3 Fischer Esterification

Fischer esterification uses and acid to catalyze the coupling of the carboxylic acid group and the alcohol group. For this reaction, the porphyrin and diol were mixed with the diol slightly less than stoichiometric ratios, to help ensure formation of the dimer instead of monoester porphyrins like in previous syntheses. These were then dissolved in toluene with an excess of tosylic acid as the catalyst. An excess is require because the nitrogen groups on the porphyrin are basic and must be fully protonated before there can be enough free acid in solution for catalysis. The reaction was refluxed with the use of a dean-stark trap to remove generated water and recycle the toluene solvent back into the reaction. This reflux could last up to several days as the esterification is quite slow, reaction progress can be tracked with TLC on the reaction periodically.

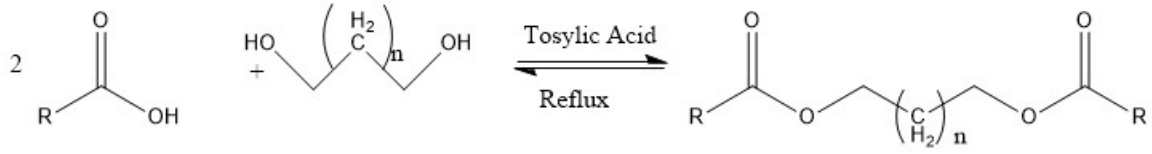

Figure 2.3: Fischer Esterification Reaction

Monoester was synthesized from TTPa and 1,9-nonanediol. ESI mass spectrum shows an M^{+1} peak of 843 amu with ESI-MS. ^{1}H NMR (300 MHz, $CDCl_3$) δ 8.79 (8H, s), 8.01 (8H, d), 7.49 (8H, d), 3.58 (6H, overlap) 1.18 (16H, overlap).

2.1.4.4 EDC Coupled Amidation

After much work on trying to make a side bridge using esters showed that synthesis to be rather difficult, the use of amides was chosen as an easier alternative. 1-Ethyl-3-(3-dimethylaminopropyl)carbodiimide (EDC) is a peptide coupling agent like the DCC that was used for steglich esterification. The mechanism of action is much the same in this case as well. The EDC reacts with the acid group to make a reactive intermediate.

While amidation happens fast with this intermediate, the intermediate is itself very unstable and breaks down rapidly. To increase the yield, a secondary coupler, N-hydroxysuccinimide (NHS) is used. NHS reacts very rapidly with the EDC-acid intermediate to make a much more stable but still reactive NHS ester compound. The amine then has more than enough time to react with the NHS ester to make the amide.

The procedure for this synthesis was adapted from a procedure by Vivero-Escoto et al.[50] A multistep process for the synthesis of the dyad creation a single amide porphyrin species intermediate over a direct synthesis as this seemed to have greater yields. The first step was to synthesis the NHS ester from TTPa. Between 10-50 mg of TTPa was dissolved in 2 mL of dichloromethane. To this solution 1.5 mol equivalent of dimethylaminopyridine (DMAP) was added. This solution was placed in an ice bath stirring. A second solution of EDC was prepared using 2.5 mol equivalents of EDC to TTPa in 2 mL of dry dimethyl sulfoxide (DMSO). Heating the solution was needed to ensure complete dissolution of the EDC. This solution was then added to the TTPa solution. Five minutes after the addition of the EDC solution, 3.75 mol equivalents of NHS. This entire solution was kept mixing on the ice bath for 4 h after which is was removed from the ice bath and left mixing at room temperature for a further 48 h.

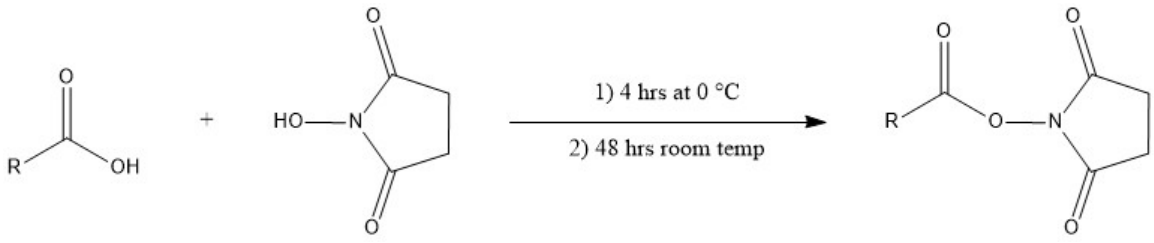

Figure 2.4: EDC Coupled reaction of TTPa and NHS to form NHS ester

The next step was to convert the NHS ester to the amide. A large excess of amine was used at this step to fully react with the NHS ester to single amide porphyrin with a

terminal free amine still free. After the NHS ester has completed reacting, the dichloromethane is removed from the reaction mixture using a rotary evaporator while the much less volatile DMSO is left behind. 3 mol equivalents of the diamine with the desired length carbon chain is then added to this mixture. The amine and the NHS ester are then reacted at 85 °C using an oil bath for 48 h. While this reaction is running, another reaction of NHS ester was run using the same starting amount of TTPa so that more was available following the completion of the monoamide porphyrin species for the end of the reaction.

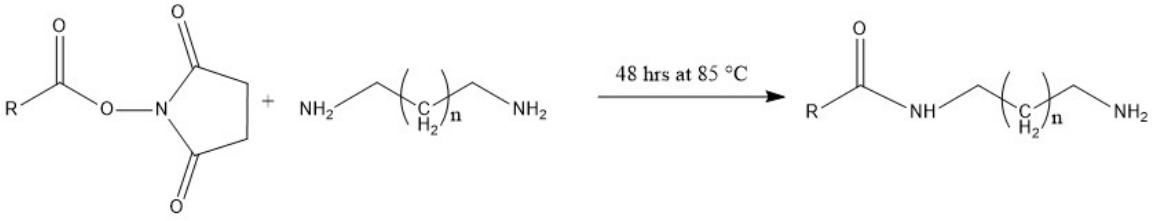

Figure 2.5: Reaction of TTPa NHS ester with diamine to make TTPA monoamide

After the reaction was completed, several milliliters of DCM was added to the reaction mixture along with several microliters of diisopropylethylamine to function as a base to deprotonate the porphyrin. The reaction was then washed with water in a separatory funnel to remove the remaining diamine from the solution. The heavier DCM settled to the bottom and was removed. If the water layer on top appeared significantly red, more diisopropylethylamine was added. The water layer was washed repeatedly with DCM until the DCM wash was colorless. All DCM was then removed by rotary evaporation

The dried monoamide species was then dissolved in DMSO and combined with the second batch of TTPa NHS ester. This reaction was heated for a further 48 h at 85 °C using an oil bath to produce the porphyrin dyad.

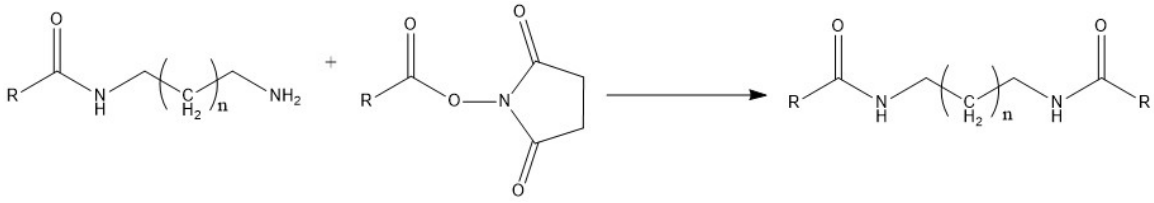

Figure 2.6: Reaction of TTPa monoamide and TTPa NHS ester to make full diamide side-bridge

The final reaction mixture was washed with water in a separatory funnel following the same procedure as before to remove the DMSO and other polar byproducts of the reaction. The porphyrin mixture was then dried using rotary evaporation. It was then purified using silica gel column chromatography with chloroform as the eluting solvent.

8 carbon side bridge was synthesized using TTPa and diaminoctane. The highest yield for this reaction is 14% of purple crystals. ESI mass spectrum shows an M^{+1} peak of 1510 amu with ESI-MS. ^{1}H NMR (300 MHz, $CDCl_3$) δ 8.87 (16H, s), 8.02 (16H, d), 7.47 (16H, d), 6.35 (2H, s), 2.72 (overlapped, s), 1.45, 1.36, 0.81 (overlapped, m).

2.1.5 Synthesis of 4,4'-Bipyridine Cross-linked Porphyrins

Concentration studies were conducted on the first choice of cross linkers with 4,4'-bipyridine (bpy) for both the monomeric TTPa, Tetratolylporphyrin(TTP) and the sidebridged dyad TTPa. For the monomer unit, samples were prepared by taking a solution of zinc metallated porphyrin, using potassium hydroxide for the TTPa but not the TTP, titration it with varying amounts of a solution of 4,4'-bipyridine. The solutions represented a range of mole ratios of bipyridine:ZnTTPa. The same procedure was used for the side-bridged dyad. These samples were left to sit for at least a day to ensure the system had reached equilibrium.

The optimal ratio for TTP and bipyridine was synthesized in the optimal ratio from the titration for NMR. ^{1}H NMR (300 MHz, $CDCl_3$) δ 8.89 (16H, s), 8.05 (16H, d), 7.53 (16H, d), 5.78 (4H, d), 2.73 (18H, s), 2.48 (4H, d).

2.2 Characterization Techniques

2.2.1 Nuclear Magnetic Resonance Spectroscopy

NMR has been a useful technique to try and analyze the products of the side bridge reactions and to examine the purity of some samples. Two different NMR machines were used for these experiments, a JOEL 300 MHz NMR and a JOEL 500 MHz NMR. 1-dimensioal H^1 and decoupled C^{13} scans were the only types of scans used for this characterization.

2.2.2 Electro-spray Ionization Mass Spectrometry

ESI-MS can be used in conjunction with NMR to help confirm the identity of products from the side bridge reaction. The instrument used was a Thermo Scientific MSQ PLUS mass spectrometer. Samples were prepped in methylene chloride at a concentration of 1 mg/mL. These samples were then diluted by a factor of 10,000:1 using a solution of formic acid in methylene chloride. The formic acid serves to protonate and therefore ionize the porphyrins for the ESI. Mass spectra were then collected for positive ions.

2.2.3 UV-Vis Absorbance Spectroscopy

UV-Vis Absorbance Spectrometry was conducted using one of two different absorbance spectrometers depending on the purpose of the scans. Quick test scans on samples were conducted using Varian Cary 50 Bio spectrometer. This single beam instrument is useful for quick scans that do not have to be as detailed, like confirming

metallation of porphyrins or checking purity of a sample. More detailed scans were run using the dual beam Varian Cary 5000 using the "slow" scan setting of the instrument from a range of 350-650 nm. This technique was used for nearly all samples of porphyrins for this project, being a basic part of the characterization of a porphyrin sample. It was also used to look at the bipyridine concentration studies by monitoring the shift in peak positions at varying concentrations of bipyridine.

2.2.4 Steady State Photoluminescence Spectroscopy

Like with the UV-Vis experiments, two different spectrometers were used. For quick characterization, emission scans, a Cary Eclipse Fluorescence Spectrometer was used on the "slow" setting and an excitation corresponding to the peak position of the soret band from the absorbance data. For the more detailed experimental scans the Jobin-Yvon Fluorolog 3 with a Hamamatsu R928 PMT detector, with excitation at the peak position of the soret band and 1 second integration time over a range of 450 to 750 nm. Slit widths for both excitation and emission were kept at 1 nm. This instrument was used for calculation of relative quantum yields, and for the bipyridine concentration studies.

2.2.5 Temperature Dependent Time Resolved Fluorescence Spectroscopy

Time resolved fluorescence of ZnTTPa and the bipyridine dimer and future dimer studies was conducted to probe the possible splitting of excited states. Samples were dissolved in a glass forming solvent made from 2 parts diethyl ether to 1 part ethanol to 1 part toluene and were mounted in a bespoke Janis ST-500 cryostat. A small bubble was left in the sample chamber which allowed the user to see if the sample remained in the cryostat after vacuum was applied. Without the bubble, it was very difficult to tell the difference between the sample and vacuum if the seals were not perfect and the sample

was vacuumed out until the scans were started. A Lakeshore 331 temperature controller regulated the temperature within the cryostat which was cooled by liquid nitrogen.

The time resolved PL scans were used with a home-built set up using a Spectra-Physics Mai-Tai HP Ti-Sapphire laser. The principal wavelength of the Laser was modified from IR to optical wavelengths using a Spectra-Physics Inspire Auto 100 OPO. Pulse modulation was achieved by two Con-Optics 350-105 modulators placed in series. PL light from the sample was collected in a front facing configuration from the cryostat and detected by a Spectral Products CM 112 double monochrometer coupled to a HPM-100 hybrid PMT. Spectra were collected in reverse mode at the peak emission wavelength for the sample with a TAC range of either 50 or 100 ns. Experiments were run from 80K to 290 K moving in 15K increments. Other scans were run with the same set up but simultaneously collect 50 ns and 674 ns windows.

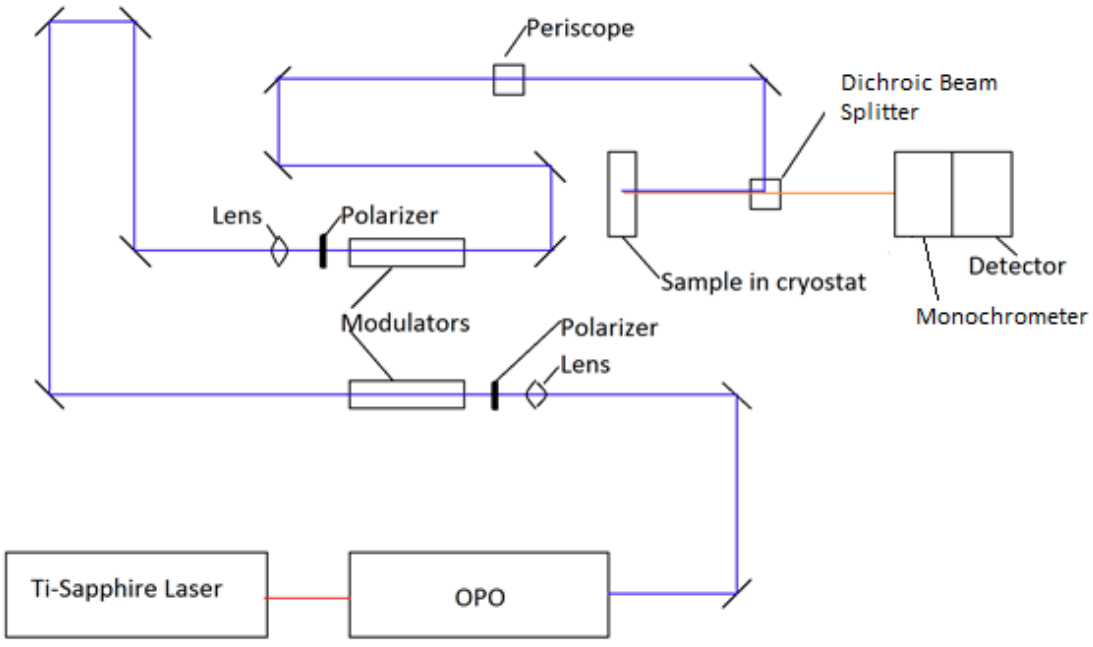

Figure 2.7: Diagram of the home-made laser set up for TRPL

CHAPTER 3: RESULTS AND DISCUSSION

3.1 Metallation of TTPa

Following the metallation of TTPa, the completion of the reaction can be confirmed quickly by UV-Vis absorbance or fluorescence data. With the absorbance scan, the soret band only shifts by a few nanometers however there are noticeable difference in the Q-bands, the number of which reduce from 4 to 2 upon metallation which can be seen below in figure 3.1. The PL spectrum looks much the same as the non-metallated spectrum but the peaks blueshift, with the primary peak shifting from 1.9 eV to 2.05 eV seen earlier in figure 1.13. Average lifetimes of the PL also decrease dramatically in time resolved experiments, dropping from 8.00 ns for the free base porphyrin to 1.88 ns for the metallated species.

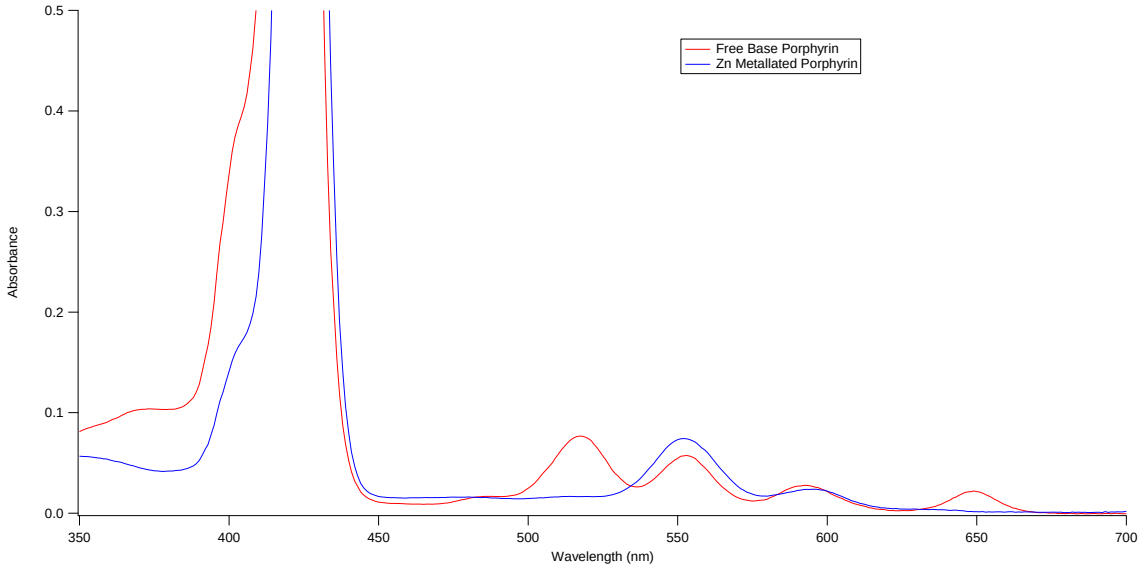

Figure 3.1: Absorbance spectrum for free base and zinc metallated TTPa

3.2 Characterization of Side Bride Reactions

3.2.1 Acyl Chloride Esterification

For the Acyl Chloride reaction, no identifiable products were obtained in enough yield for NMR analysis. Column chromatography revealed a large number of bands that were eluted. This would indicate that this synthesis is not very selective and many products that are not desired were obtained. While many of these bands were still characteristically porphyrins as revealed by UV-Vis and PL data, Mass spec revealed a range of mass to charge values ranging from 700 which is the weight of TTPa all the way up to 1700 with no peaks corresponding to the desired diester bridge or even the monoester products. Repeating this synthesis several times showed the same result, so it was decided this method was not the best direction for synthesis because of its apparent poor selectivity, leading to the exploration of other methods

3.2.2 Steglich Esterification

This method initially looked far more promising in terms of selectivity. Only two bands eluted from the column, with a third, very faint, immobile band at the very top of the silica gel. The first band confirmed by NMR was shown to be just unreacted TTPa. The NMR of the second band to elute was more interesting. Seen below in figure 3.2 it shows that the DCC is still bound to the porphyrin. DCC intermediates can undergo a chemical rearrangement to the N-acylurea of DCC and TTPa. This rearrangement is slow and would only occur if the esterification reaction was even slower. This indicates that this reaction is also probably not good route for the ester based side bridge. There is also excess DCC still present.

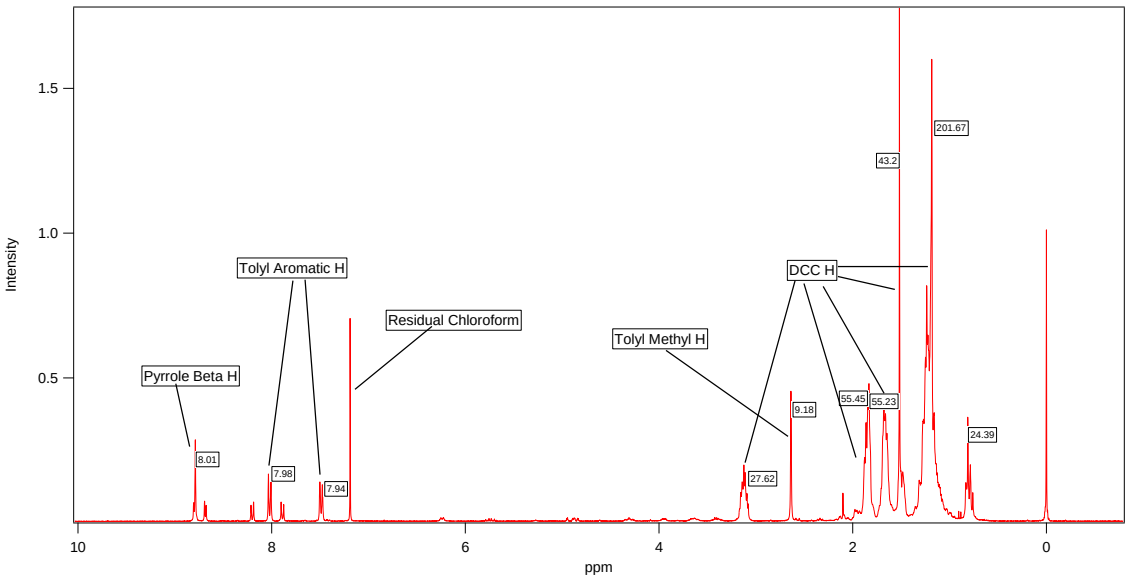

Figure 3.2: NMR spectrum of Steglich esterification product. Peaks around 8pmm correspond to the porphyrin hydrogens. Peaks from 1 to 3 are identical to DCC NMR spectrum. Relative integrals listed by peaks

3.2.3 Fischer Esterification

The Fischer esterification reaction shows the most promise as a synthesis method for the ester side bridge. NMR confirmed the addition of 1,9-nonanediol to the porphyrin, however resulting integration of peaks so integration ratios corresponding to the formation of only a single ester bond, not the formation of dimer. Mass spec confirmed a mass to charge ratio of 843 corresponding to the monoester product. This is promising result however this reaction is plagued with a problem. Like the acyl chloride synthesis, there were many bands on the column, most were very well retained and almost impossible to elute. Not all the bands appeared to be porphyrins though, with significant changes in the fluorescence and UV-Vis properties that were no longer characteristic of porphyrins. A possibility is that the acidic conditions of the reaction and maintaining a high temperature for several days caused the porphyrin ring to decompose.

However running this reaction at higher concentrations in multiple steps might mean it can spend less time at high temperatures and increase the yields.

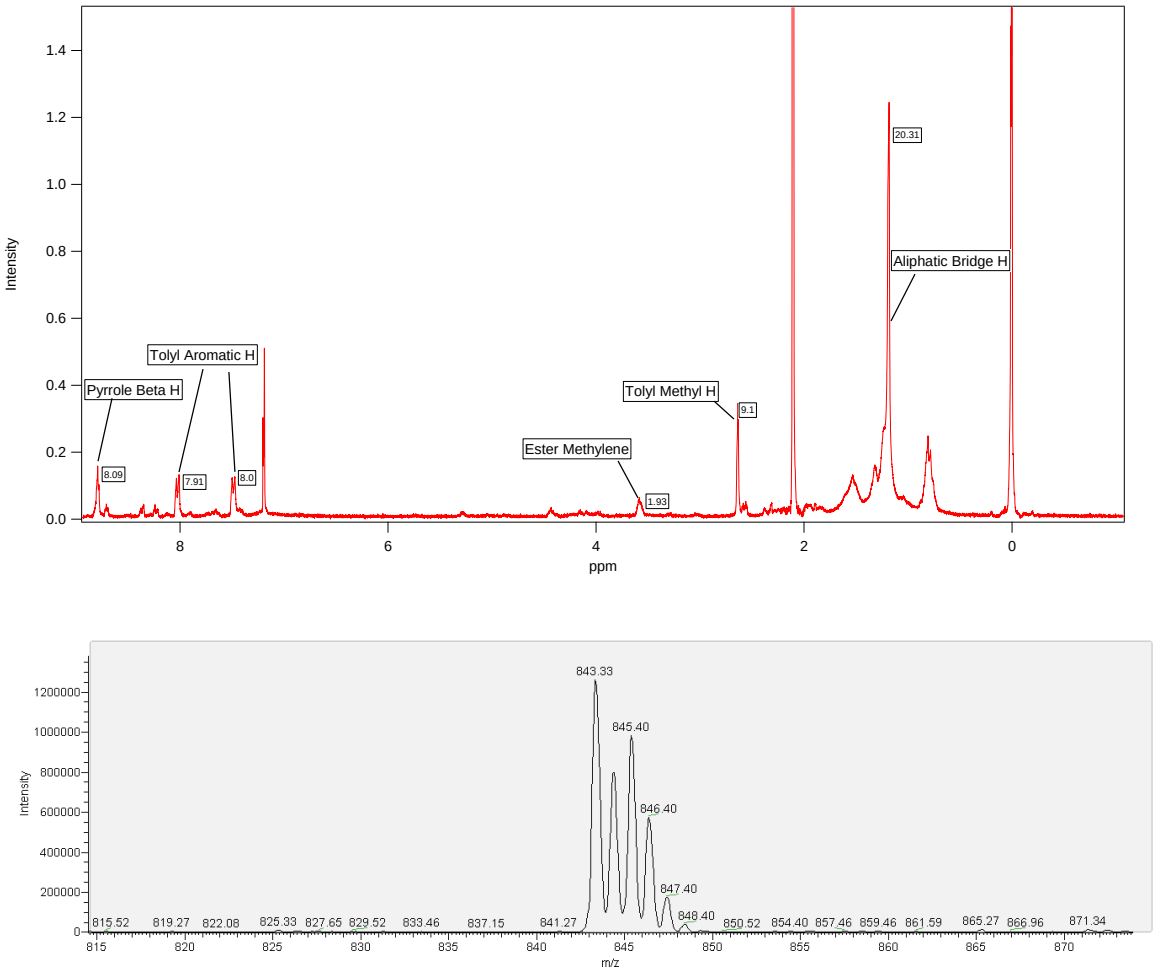

Figure 3.3: top: proton NMR spectrum of Fischer esterification product. Bottom: mass spectrum of Fischer esterification product. Relative Intergrals listed next to peaks

3.2.4 EDC coupled Amidation

The EDC coupled reaction was shown to still have some issues in regards to yields but is capable of successful synthesis of the carbon bridged dyad. Mass spectrometry was used to confirm the product showing a mass of 1510 amu corresponding to the 8 carbon sidebridge porphyrin dyad. Additionally NMR and IR Spectra of the compound was obtained. Yields remain low however, and have been shown to drop off dramatically as the synthesis is scaled up. From 10 mg of starting

TTPa, 1.7 mg of product was recovered. From 25 mg of starting TTPa however, 0.5 mg of product were recovered. Scaling up to 120 mg of TTPa, no measurable amount of product was recovered. In this reaction, there are many unwanted side products that seem to be possible. During purification, around 8 distinct bands can be eluted from the column indicating other products. It is hypothesized that at higher concentrations of the reaction, these side reactions become more probable and are out competing the desired reaction. One possible reaction is the rearrangement of the EDC o-acylurea intermediate to the stable N-acylurea. These side reactions might be avoided in future reactions by adding more solvent to lower the concentration and also experimenting with shorting heating times on the oil bath.

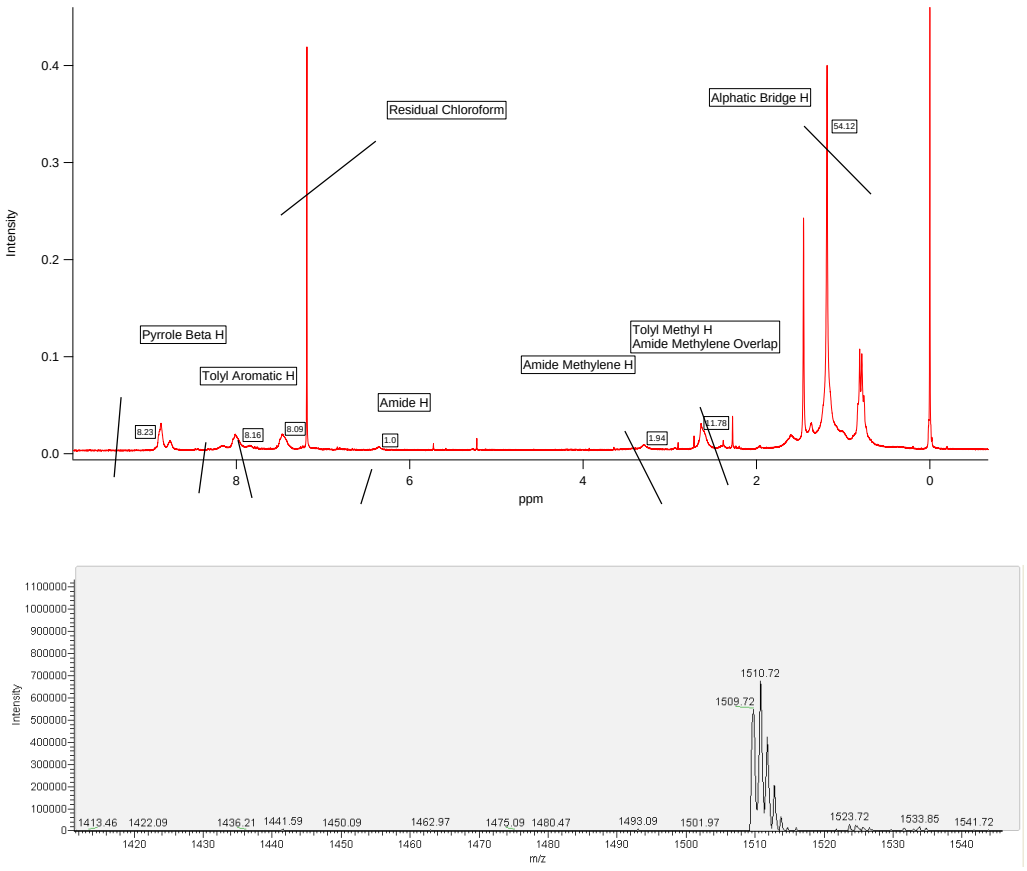

Figure 3.4 top: proton NMR spectrum of the 8 carbon side chain dyad, bottom mass spectrum of the porphyrin dyad. Relative Integrals are listed next to peaks

In figure 3.4, porphyrin and aromatic tolyl hydrogens can be seen in the 8 ppm and higher region. The large singlet peak at 7 ppm corresponds to residual chloroform in the NMR solvent. The amide hydrogens can be seen as a broad peak at 6.5 ppm. The methyl moiety of the tolyl group and the carbons of the side chain can be seen between 2 1 and 3 ppm. Small trace impurity peaks can be seen between 5 and 6 ppm that could not be reduced with further purification steps.

3.3 4,4'-Bipyridine Concentration Studies

3.3.1 TTPa Concentration Studies

Samples that contain mixtures of bipyridine to ZnTTPa in varying mole ratios were prepare as discussed earlier. These samples were then characterized using UV-Vis, photoluminescence. The results are shown below in figure 3.5. The absorbance data shows a red shift in all peaks of the absorption spectrum, the soret band is the focus of the figure 3.5 because of the higher detail for the examination of finer features. It can be seen in the soret peak that the peak at 420 nm in the control gradually diminishes as a new feature grow in at 435nm. This peak at 435 nm reaches a maximum at a mole ratio of 1:1 after which is starts to decrease again. The same trend was seen in the PL data where the emission peaks shift by about 15 meV at a mole ratio of 1:1. At higher mole ratios the peaks shift back to their original positions.

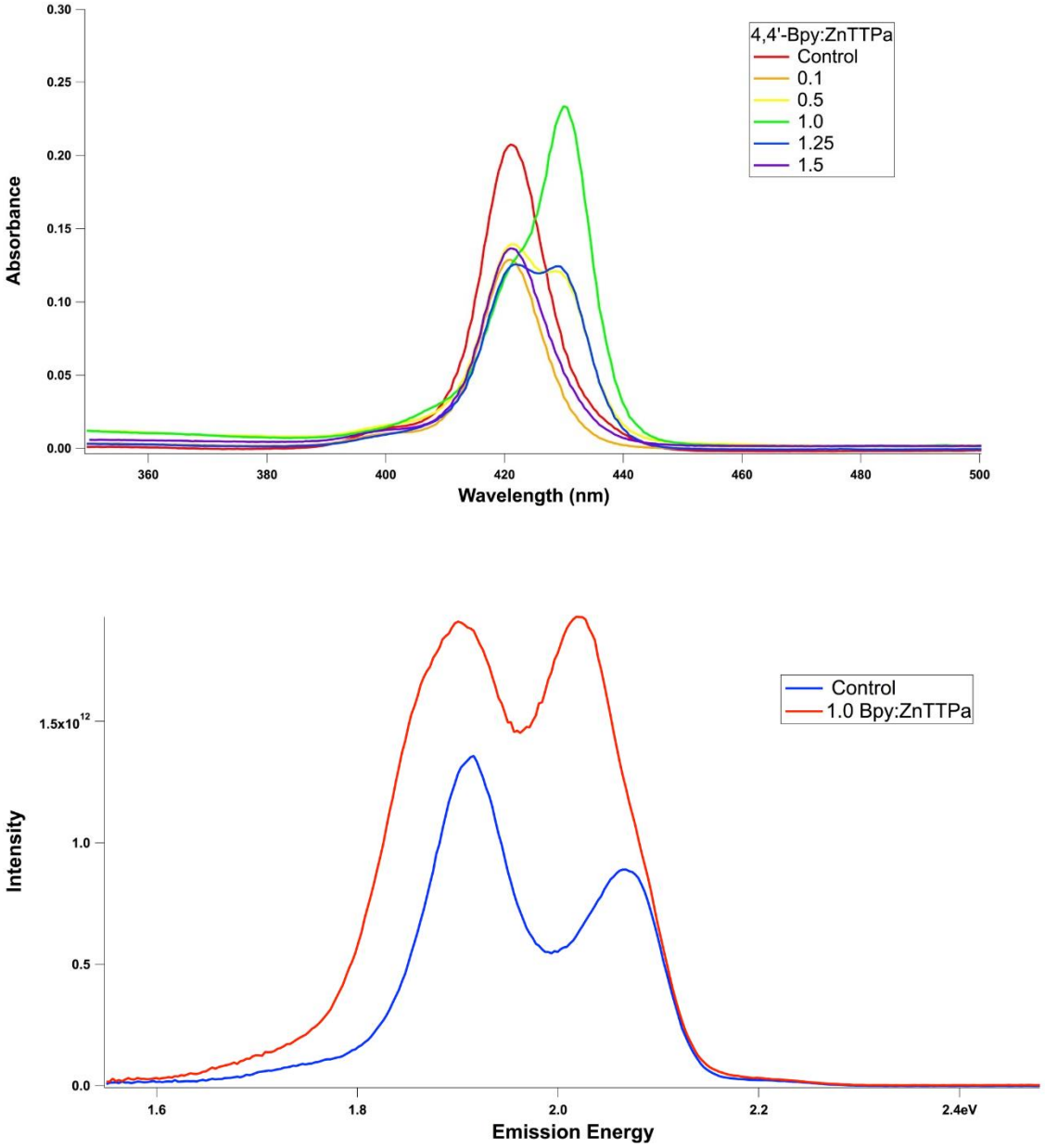

Figure 3.5: Top: Absorbance of the Soret peak at varying ratios of 4,4'-bipyridine:ZnTTPa. Bottom: PL data of the control vs 1:1 4,4'-bipyridine:ZnTTPa. Other scans were removed to make the shift more apparent.

The data does seem to show something occurs to the samples with the addition of 4,4'-bipyridine that has an optimum at the aforementioned 1:1 ratio. At higher ratios, the

spectra return to looking the same as the control. This is not definitive proof of the formation of dimers, but it is compelling evidence for that possibility.

The reason why there is an optimum ratio like this, and it is not possible to just add an excess of bipyridine to drive the formation of a dimer to completion is that in excess, every porphyrin will be already bound to a bipyridine. This means that there are no free porphyrins to bind left to bind for the dimers. So at high concentrations you have the monomeric ZnTTPa bipyridine species dominating the spectrum, which will appear indistinguishable from unbound ZnTTPa on these spectra. So the behavior is reflective of dimer formation. Due to this, one would expect the ideal mole ratio of the dimer to be 0.5:1 bipyridine:ZnTTPa. The reason this might not be the case in reality is that the bipyridine might not be the most strongly bound choice for a ligand, so it takes an excess to drive the dimer formation. Another possibility for this is that the solutions were not completely scrubbed of all acidic conditions by the potassium hydroxide, which would mean some of the bipyridine would be protonated, and the excess is neutralizing the solution.

The other issue that needs to be addressed with this data is that it does not show the expected blue-shift in absorption and emission that one would expect in the presence of the coupling to the transition dipoles. If this data is indeed representative of the formation of the dimer, then the most probably explanation would seem to be that this system is free to rotate. The strong coupling of the transition dipoles requires a parallel alignment and the true alignment of this system is a different confirmation. While it is not strong enough data to draw firm conclusions on at this point, it is worth noting that

there is a blue-shifted shoulder on the 1:1 ratio samples soret band that might represent a small population of dimers that could have a more ideal transition dipole alignment.

3.3.2 TTP Concentration Studies

Concentration studies were performed to explore binding between bipyridine and the tetratolyl porphyrin (TTP). Solutions of the porphyrin dyad, combined in varying ratios, were characterized by UV-vis and steady state photoluminescence experiments. The change in relative quantum yields at different mole ratios of the titration can be seen below in figure 3.6

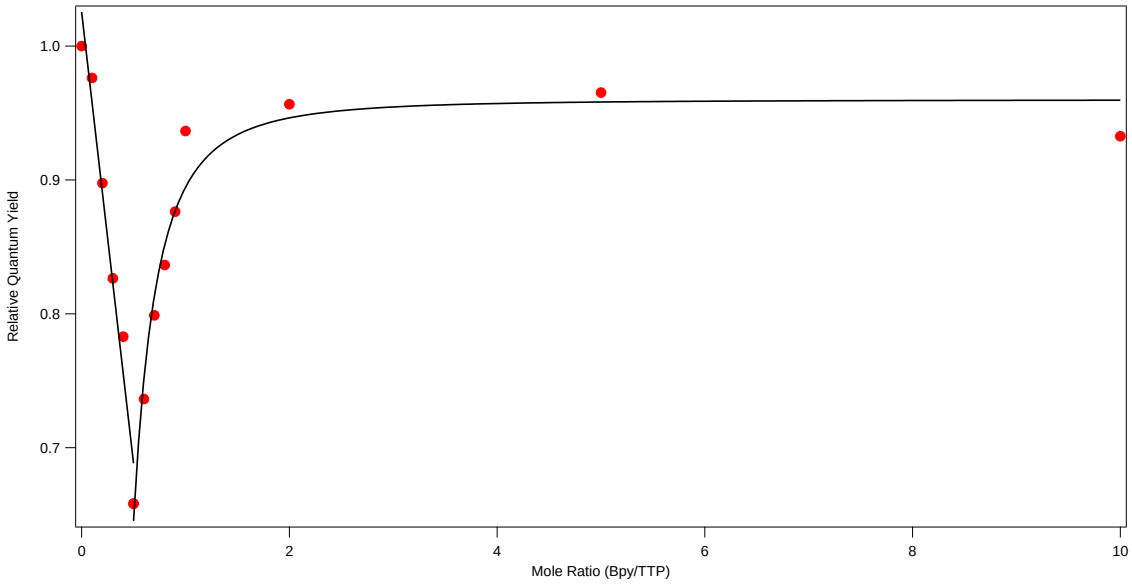

Figure 3.6 Relative quantum yields of different ratios of bpy:TTP compared to the quantum yield with no bipyridine

The quantum yields show a very distinct minimum at a ratio of 0.5:1 bpy:TTP, This minimum corresponds to the formation of a coupled dimer whose quantum efficiency is being quenched by the formation of a dark excited state. Past the mole ratio of 0.5:1 the efficiency starts to increase again, as the solution is now over titrated with bipyridine. This leads to the formation of TTP/Bpy monomers with no coupling rather than dimers with coupling. By a mole ratio of 1:1 the quantum yields have leveled off.

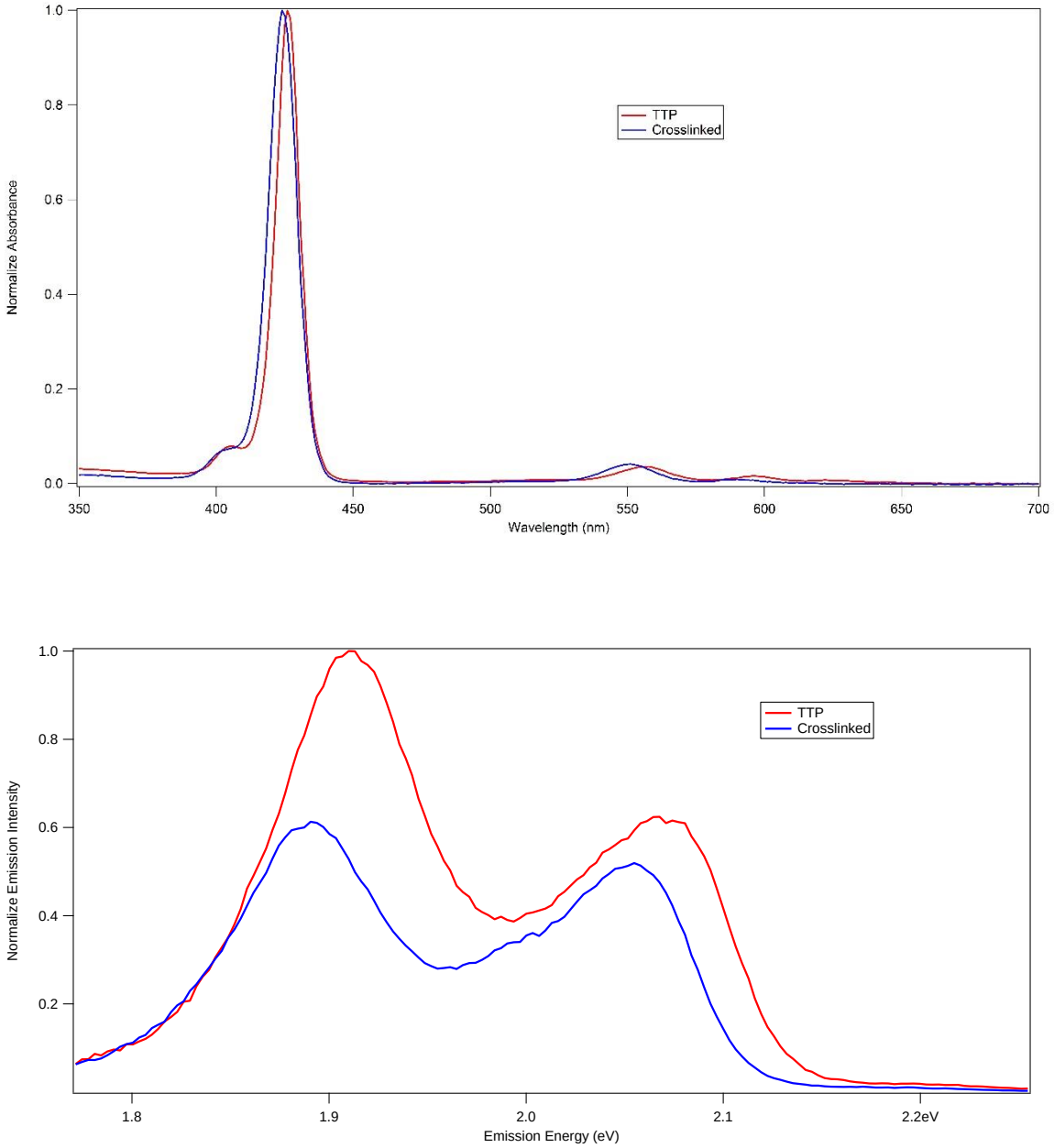

Figure 3.7 Top: Normalized Absorption spectra of the soret peak of TTP and Cross-linked TTP. Bottom: PL emission spectra of the same ratios

The behavior of the steady state data show the expected blue shift for the UV-Vis

The UV-Vis data shows a shift of 2 nm or 21 meV at the soret peak. The steady state PL

actually shows a red shift of 19.3 meV. If the coupling is weak it is possible that the emission might actually be seen out of the lower energy coupled excited states. Even if the emission is weaker from this state, it should have a significantly higher population than the higher level excited state. There the redshift of the PL would be equal equal in magnitude to the blue shift of the absorption spectrum. This shift would be equal to J_{12} splitting from the model. The splitting of the excited states would be equal to $2J_{12}$ or 38.6 meV from the PL data for this system (figure 3.7)

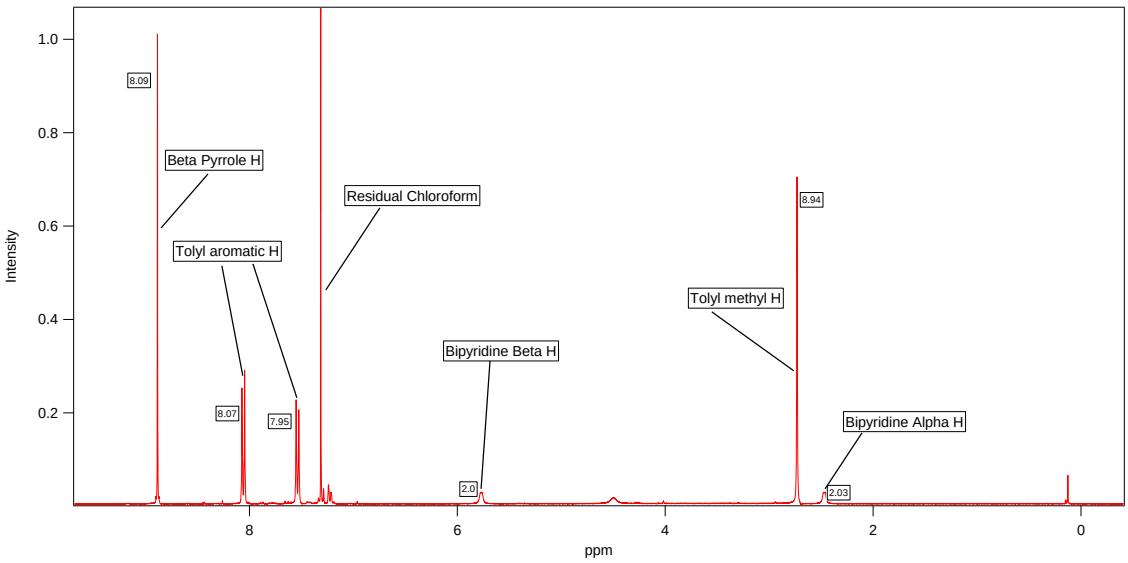

Figure 3.8 NMR spectrum of TTP bipyridine dimer

Once the titration data was characterized, and nmr spectrum of the TTP/Bpy was obtained, seen above in figure 3.10. The alpha and beta hydrogens of the bipyidine is considerable more upfield than is the case for bipyridine on its own. This is due to strong shielding effects on these hydrogens by the delocalized porphyrin ring system in close proximity.[22, 39, 51]. This again is strong evidence of the formation of cofacial porphyrin dimers.

3.3.3 Porphyrin Dyad Concentration Studies

Concentration studies titrated were performed in the same fashion of the previous concentrations studies. Solutions the porphyrin dyad were combined in varying ratios were characterized by UV-vis and steady state photoluminescence experiments. The results can be seen below in figure 3.9.

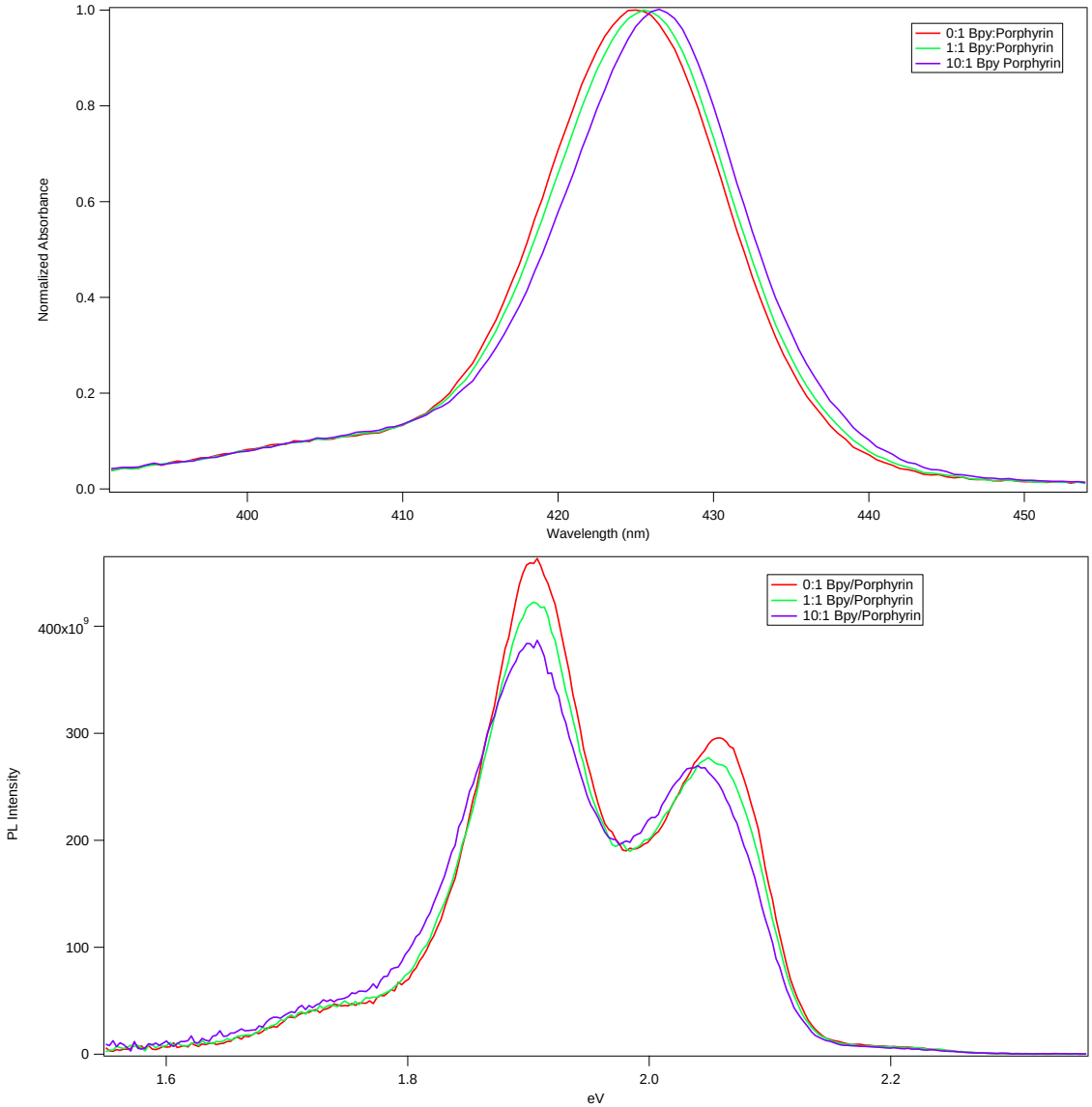

Figure 3.9 Top: Normalized Absorption spectra of the soret peak of selected ratios of bpy. Bottom: PL emission spectra of the same ratios

The data for this titration shows a gradual but continuous red shift in both absorption and emission spectra for the titration. Curve fitting the line-shape spectra of these titrations do no elucidate any addition states growing in during the titration, rather what is seen is a gradual redshift and broadening of the fit peaks already present in the spectra. To look a little further into this phenomena, relative quantum yields were plotted, seen below in figure 3.10

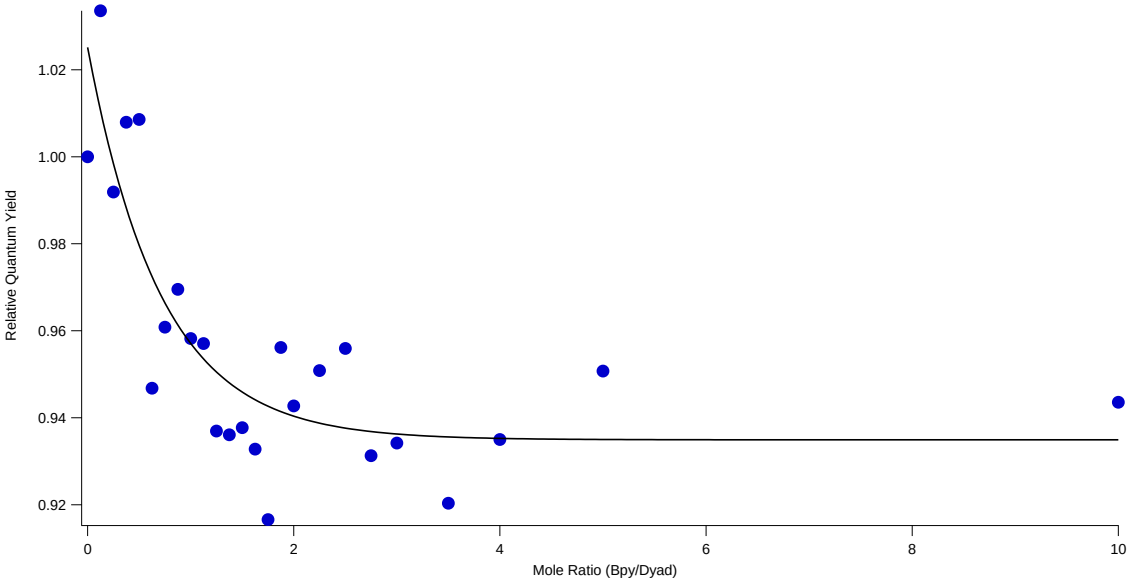

Figure 3.10 Relative quantum yields of different ratios of bpy:dyad compared to the quantum yield with no bipyridine

The relative quantum yields so a decrease of about 6% leveling off after a mole ratio between 1 to 2. The quantum yields do not follow the exact same trend as the absorption and photoluminescence spectra. While the spectra continue to redshift and broaden more and more as higher amounts of bipyridine is added, the quantum yields level off after a point and do not change after that. Instead of forming a cofacial dyad, bipyridine instead is the trigger for the formation of aggregates in solution.

Looking into causes for this, two possibilities emerge. The initial decision to go for the 8 carbon chain side bridge first was based on Spartan computations for the

porphyrin/porphyrin distance in the porphyrin bipyridine complex. Eight carbons seemed to be the best length for allowing the system to be cofacial without allowing for large amounts of rotation. Returning to Spartan, a further computation was run to examine the preferred orientation of the side bridge. This revealed the possibility that the side bridge does not orient the two porphyrin rings of the dyad in a way that is favorable for the formation of a cofacial system. Additionally the zinc-zinc spacing in the bipyridine cofacial dyad was calculated as 11.5 Å. The side bridge of 8 carbons allows for a spacing of this size. Making the more likely explanation to be an improper geometric arrangement caused by the amide bonds (figure 3.13

3.4 Temperature Controlled Photoluminescence Studies

3.4.1 Unsidebridged TTPa Study

Temperature Controlled lifetime data was taken on both the ZnTTPa molecule and the possible optimized dimer seen in the bipyridine concentration studies run in a glass forming solvent that is a mixture of diethyl ether, ethanol, and toluene in a 2:1:1 ratio with a 50 ns TAC window The results of these scans are in figure 3.8. The data decays themselves show that for the fast part of the decay a good overlap between the monomer and dimer, but for the slower parts of the curve, the dimer has a considerably longer decay compared with the monomer. An effect that is even more pronounced at lower temperatures.

Also in figure 3.11 is a plot of average emission lifetime vs temperature and a plot of emission intensity vs temperature for both monomer and dimer porphyrin. For average lifetimes, it can be seen that the average lifetime is considerable longer for the dimer than the monomer. Also the average lifetime grows considerably longer for the dimer at

colder temperatures. The monomer shows that its average lifetime shortens initially with temperature. There is however an anomaly in the plot is due to the glass transition of the solvent. The dimer also shows much less temperature dependence on emission intensity compared to the monomer.

If there is coupling happening between the two porphyrins in the dimer that is leading to the splitting of the excited states, it would be expected that the average lifetimes would be longer. More specifically there would be an extra component in the long part of the decay corresponding to excited electrons becoming trapped in a dark excited state for some time before thermal excitation moves it back into a bright state where it emits. Emission from electrons from the bright state that do not go into the dark state would have much the same appearance as emission from the monomer. This fits what we see, the fast part of the curve which would represent emission directly from the bright state in the presence of coupling matches with the monomer. However at longer delay times, there is a new component in the dimers decay that is not present for the monomer, possibly representing an electron entering and exiting a dark state.

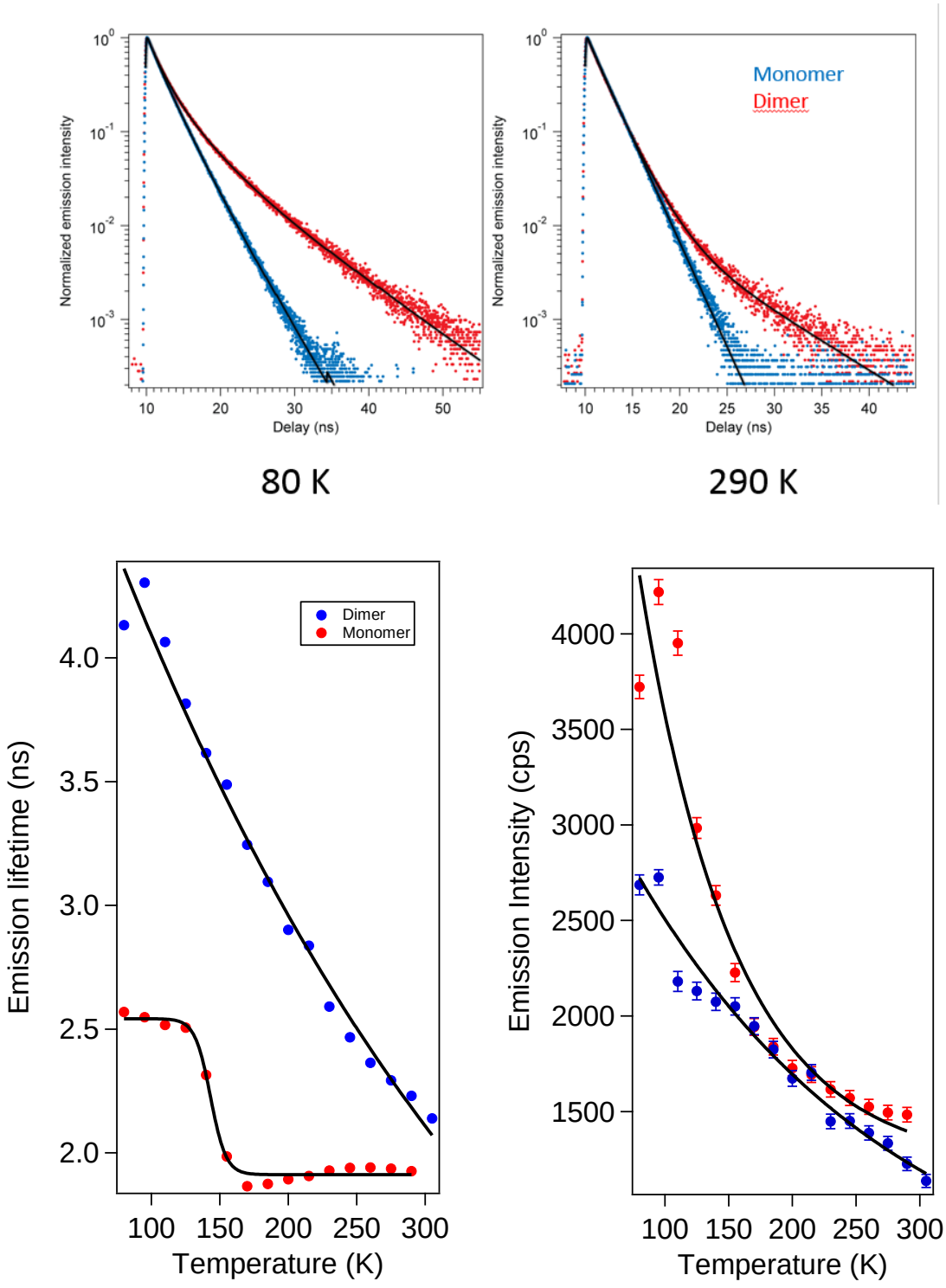

Figure 3.11: Top: PL decay histograms for monomer and dimer at 80K and 290K. Bottom Left: Emission lifetime vs temperature. Bottom right: Emission Intensity vs Temperature

Additionally, by looking at the average lifetime vs temperature plot, it can be seen that the dimer shows a significant lengthening of lifetimes for the dimer at colder temperatures. Whereas for the monomer, there is very little change except for a possible glass transition anomaly at 150K. This still fits well with the coupling model. If there is coupling we would expect the lifetime of the dimer to be considerably longer at colder temperatures as there is less thermal energy available to bring an electron back out of the dark state. The lifetime at 80K for the dimer is almost double that of the monomer.

While the lifetimes fit well with the coupling model, the earlier observed redshift in the steady state spectra suggest something else might also be happening. It is possible that the carboxylate side group that caused issues with the steady state spectra might also be effecting the coupling. It is difficult in this case to say what the splitting of excited states could be as the data does not fully support the case of transition dipole coupling.

3.4.2 TTP Study

Temperature controlled studies of the tetratolyl porphyrin were conducted to try and eliminate any issues that may be arising from the carboxylate functionality of the TTPa. 2-methyl THF was the glass forming solvent used. The decays were collected simultaneously in 50 and 674 ns TAC window. However the blue shift seen in steady state data shows a system behaving as more as we would expect the coupled system to behave. The lifetimes grow longer for the bipyridine linked dimer. The results can be seen below in figure 3.12

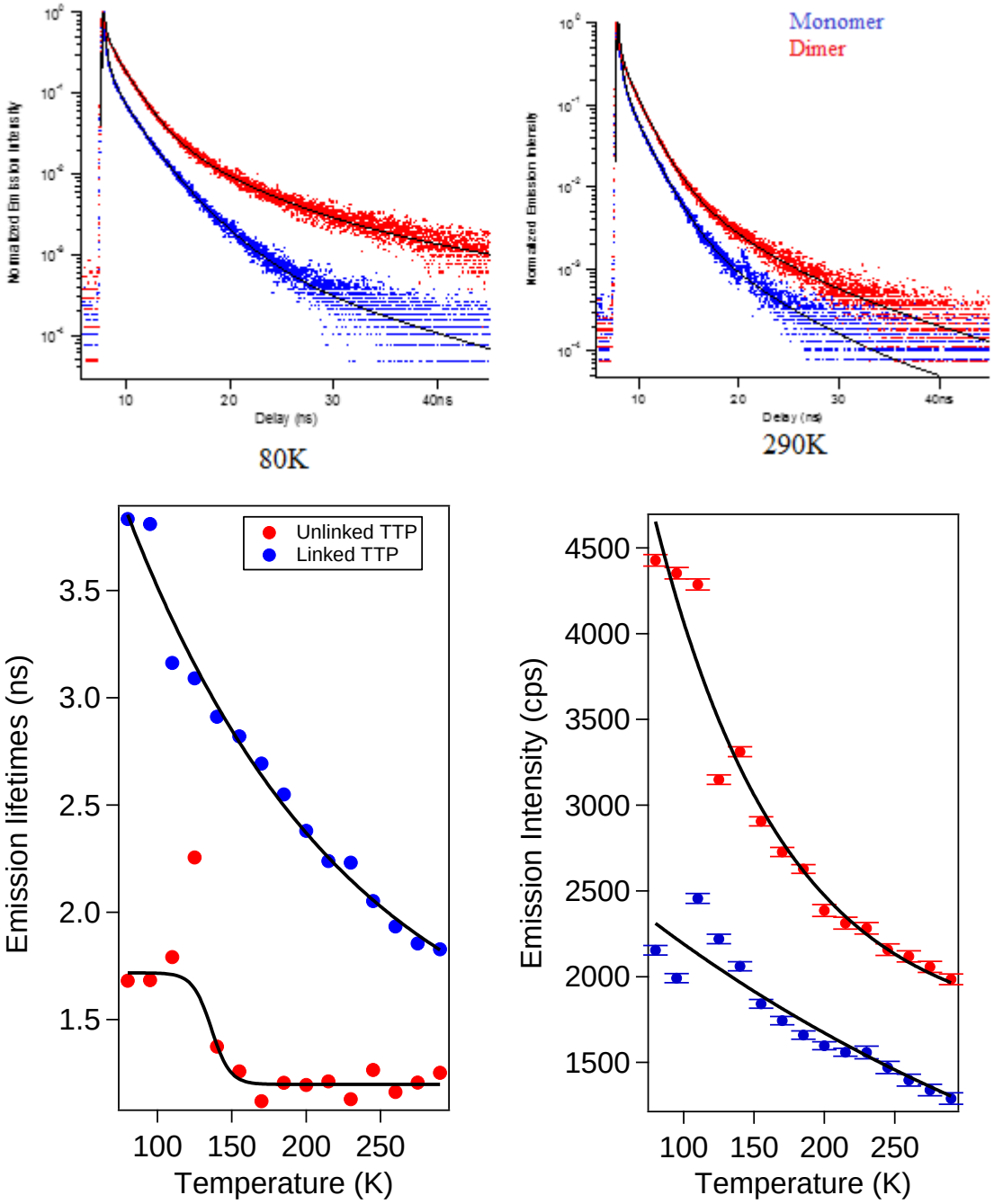

Figure 3.12 Top: PL decay histograms for monomer and dimer at 80K and 290K. Bottom: Emission lifetime vs temperature.

While the shape of the decay curves are more complex than in the case of TTPa, the tetratolyl porphyrin the trends shown are consistent with what would be expected in the presence of dipole coupling. The unlinked TTP lifetimes are fairly flat with respect to temperature, with one slight sigmoid shaped decrease around 140 K. The likely cause of

this is small effects of glass transition of the solvent 2-methyl THF, which has a glass transition at 142 K[52]. The linked TTP has much longer lifetimes than the unlinked. Additional a much more pronounced temperature dependence in decay lifetimes is apparent, from 3.8 ns at 80 K to 1.8 ns at 290 K.

We can examine the intensities at different temperatures for this data as a reflection of quantum yields at different temperatures. The plot of intensities show that temperature does have an effect on both the TTP and cross-linked TTP, with decreasing intensity at increasing temperatures. The effect is much less pronounced though for the cross-linked species changing by less than half the amount of TTP. This does not immediately agree with what would be expect from coupling. One would assume coupling more electron would be trapped in the dark state at colder temperatures, making the intensity lower than at higher temperatures. This assumption though is not complete as temperature itself has other effects that can alter quantum yields. Higher temperatures allow for additional conformations of the molecules that can lower quantum yields. To correct for this, the assumption can be made that these effects would be much the same for TTP and cross-linked TTP. Therefore the cross-linked intensity can be normalized by the intensities of monomeric TTP. These normalized intensities seen below in figure 3.13, show that the intensites actually increase with temperature. This now agrees with the case for coupling as well. Showing a temperature dependent increase in intensity for the cross-linked species.

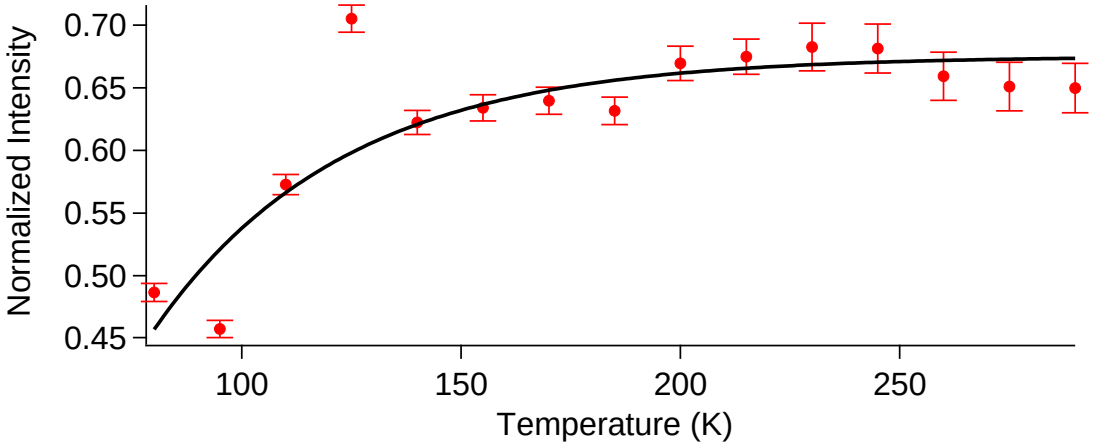

Figure 3.13 Plot of normalized intensities of cross-linked TTP vs temperature

3.4.2.1 Fitting to Boltzmann Distribution

These data combined with a clear blue shift in the steady state data strongly supports the case of dipole coupling in this system[7, 11, 13-14]. To measure the degree of coupling from the lifetime data though, the Boltzmann distribution must be used to describe the lifetime data. To start with, we assume a two state system to describe the excited states. A higher energy bright state and a lower energy dark. The Boltzmann distribution for this system is:

$$\frac{P_B}{P_D} = e^{-\Delta\varepsilon/k_b T} \qquad \text{Equation 3.1}$$

P_B and P_D are the probabilities that the bright or dark state is occupied, respectively. $\Delta\varepsilon$ is the spacing between the states, k_b is Boltzmann's constant, and T is the temperature. Since we are assuming only two states, the probabilities of both states must be add up to one. This can be rearrange with P_D in terms of P_B

$$P_B + P_D = 1 \qquad \text{Equation 3.2}$$

$$P_D = 1 - P_B \qquad \text{Equation 3.3}$$

We can then plug equation 3.3 into equation 3.1 gives a new equation in terms of the P_B. This equation can now be solved for P_B:

$$\frac{P_B}{1-P_B} = e^{-\Delta\varepsilon/k_bT} \qquad \text{Equation 3.4}$$

$$P_B = \frac{e^{-\Delta\varepsilon/k_bT}}{1+e^{-\Delta\varepsilon/k_bT}} \qquad \text{Equation 3.5}$$

If we now consider the photoluminscent decay rate (k_{PL}) for the cross-linked dimer, it can be expressed as the sums of the rates of the bright (k_{PLB}) and dark (k_{PLD}) states.

$$k_{PL} = P_D k_{PL_D} + P_B k_{PL_B} = (1 - P_B) k_{PL_D} + P_B k_{PL_B} \qquad \text{Equation 3.6}$$

Equations 3.5 and 3.6 can be combined and simplified to give the equation to describe k_{PL} as a function of temperature.

$$k_{PL}(T) = \frac{k_{PL_D}}{1+e^{-\Delta\varepsilon/k_bT}} + \frac{e^{-\Delta\varepsilon/k_bT}}{1+e^{-\Delta\varepsilon/k_bT}} k_{PL_B} \qquad \text{Equation 3.7}$$

This is now a function that can be used to describe the calculated decay rates obtained from the temperature controlled lifetimes study. Using Igor Pro as the fitting software, the experimentally obtained radiative rates were fit using equation 3.7, seen below in figure 3.14.

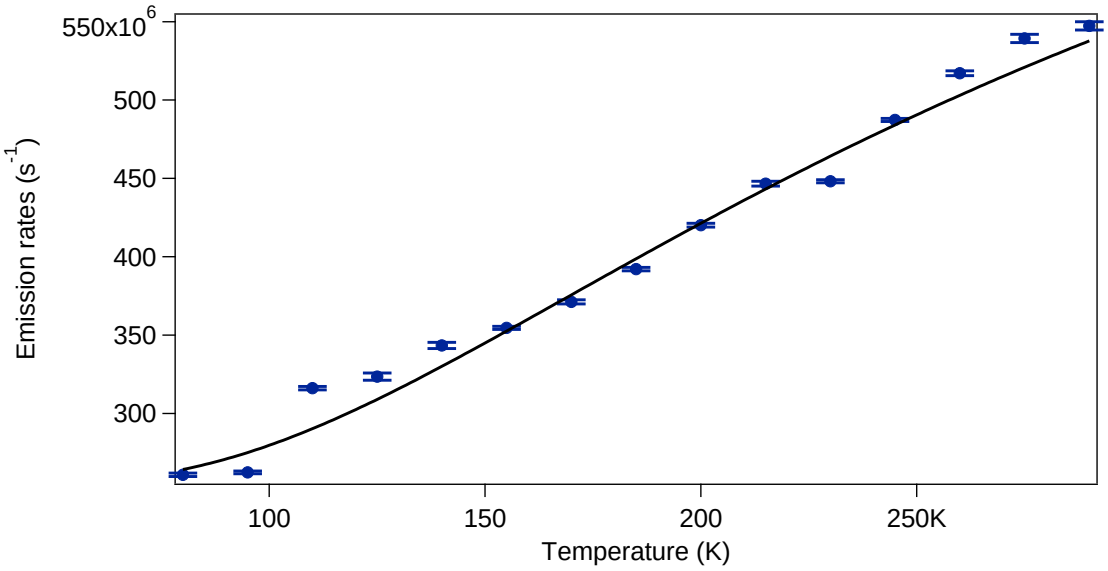

Figure 3.14 Plot of emission rates vs temperature with the fit function of these data as the black line

The curve fitting of the data yields the values for the coefficients as $k_{PLB} = 1.67 \times 10^9 \pm 0.02 \times 10^9\ s^{-1}$, $k_{PLD} = 2.55 \times 10^8 \pm .10 \times 10^8\ s^{-1}$, and lastly the energy spacing of the two states, $\Delta\varepsilon = 34.8 \pm .3$ meV. This spacing is in very good agreement with the data from the steady state data, from which the PL scans gave a value of 38.6 meV. This value is significantly higher than the value of k_bT at room temperature of 25.7 meV. This would explain why the average lifetimes do not level off, but are still sharply decreasing at 290 K.

3.4.3 Side bridged TTPa study

Temperature controlled studies on the 8 carbon side bridged dimer in 2-methyl THF as the glass form solvent. The data from these studies further support the data from the steady state experiments that no coupling seems to be occurring with this compound. The data from this study can be seen below in figure 3.14

The lifetimes for this compound show very little different between the linked and unlinked. At 80 kelvin the lifetimes are 2.35 and 2.55 ns for without bipyridine and with

bipyridine samples respectively. At 290 kelvin the lifetimes are 1.37 and 1.69 for without bipyridine and with bipyridine samples respectively. Whereas before the differences between the two samples was quite large at low temperatures, in this case, the differences are quite small. Additionally the sample with bipyridine shows only a slight change with respect to temperature instead of a quite marked difference in the previous two cases. Both the trends follow a sigmoidal pattern with an inflection around the same temperature as the glass transition of the solvent. The bipyridine linked dyad does so some degree of long components in the lifetimes, but these values are quite small and have little contribution to the average lifetime. This evidence supports the conclusions from the steady state data that the dyad does seems to be forming random aggregates instead of cofacial dimers. Intermolecular linked of porphyrin rings might align some of the transition dipoles favorably, which would explain the small long components in the decays.

The lifetimes of this compound both with and without bipyridine show an additional puzzle not present in the unsidebridged case. Lifetime fitting of the decay curves could not be achieved without a negative decay component. These negative components were fairly short ranging in the first 100 picoseconds of the decay. This negative component is a sign of energy transfer within the system. This is a quite puzzling mystery as there is not an obvious cause for why energy transfer should be observed in this system. A possibility is that the dyads aggregate in solution, allowing for energy transfer within the aggregates. The addition of bipyridine seems to slightly alter the characteristics of the aggregates, seen in the redshifted spectrum and the slightly different PL decays, but the effect of energy transfer is unchanged.

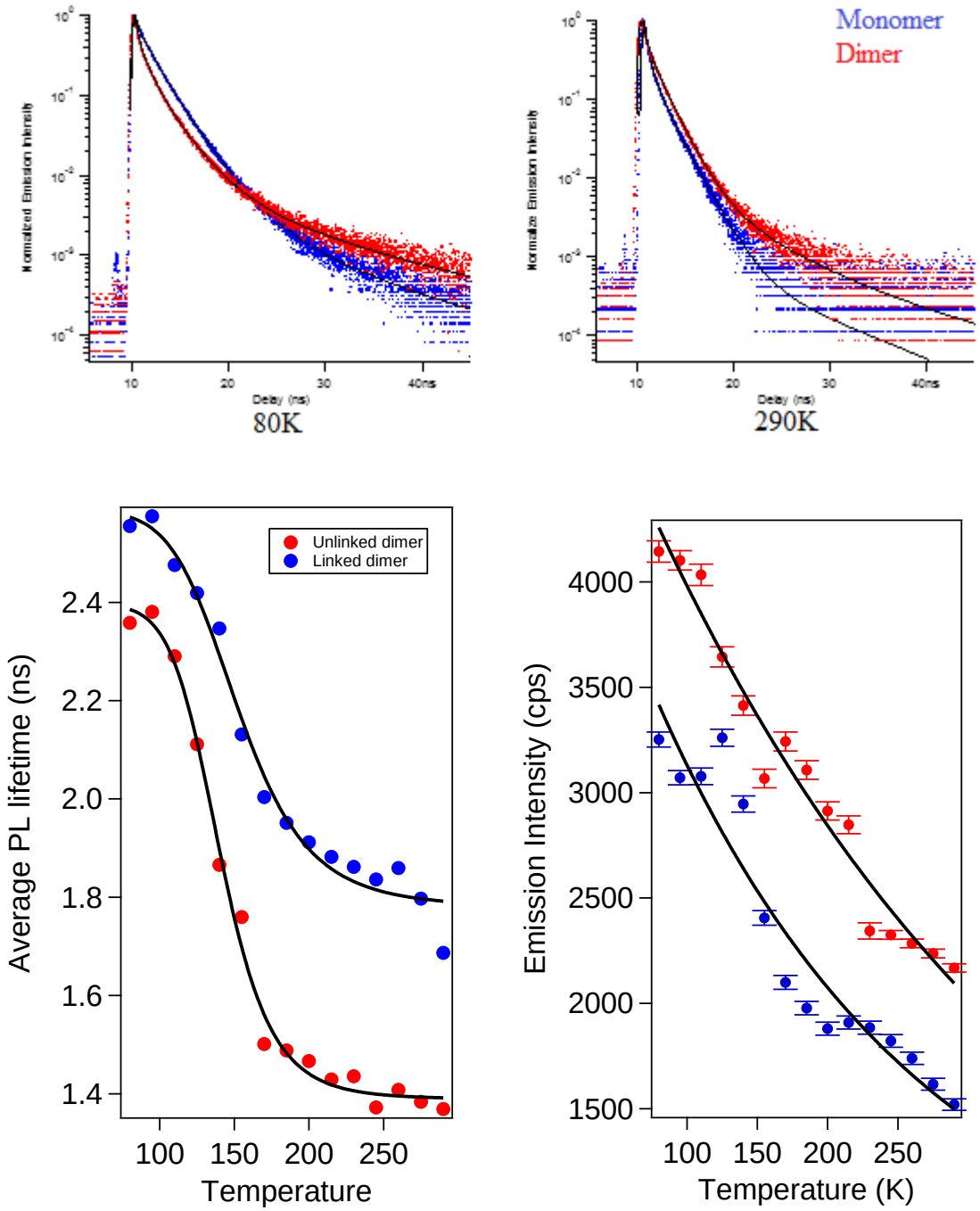

Figure 3.14: Top: PL decay histograms for monomer and dimer at 80K and 290K. Bottom: Emission lifetime vs temperature.

Looking at the intensities for the unlinked and cross-linked, the intensities of the cross-linked species is clearly lower. However, the temperature dependence of both species look much the same. The difference in intensity of the two with respect to temperature is more or less constant. This is consistent with a lack of any coupling in the presence of bipyridine.

3.5 Computations on Porphyrin Dyad

Due to the unexpected results from the steady state and lifetime data, it is clear that something else was occurring at the molecular level. To explore this further, more focused Spartan calculations were conducted on the dyad system. The original calculations were conducted using semi-empirical computations on the bipyridine linked system in order to determine the ideal side bridge length. The eight carbon chain is a perfect fit for the bipyridine dimers, allowing for an inter-ring spacing of 11.5 Å. The density function calculations show this spacing is still ideal, if the side bridge is perfectly aligned.

Looking to the orientation of the side bridge, the bipyridine was removed and the orientation of the side bridge relative to the amide bond was explored using computations. Due to resonance of amide systems, amide bonds are fairly rigid and can adopt two possible orientations. Seen below in figure 3.15, the two possible confirmations of the side bridge. The orientation of the ideal alignment for our system, where the side bridge lies 90° to the porphyrin ring was not the ideal configuration in Spartan simulations. Instead an orientation where the side bridge is nearly 0° to the porphyrin ring, extending off the side.

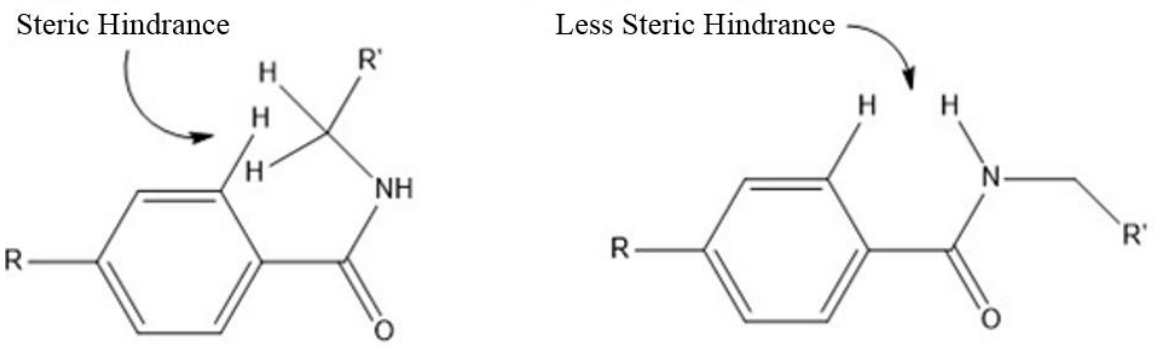

Figure 3.15 The two possible orientations of the amide side bridge bond.

As figure 3.13 shows, the reason why the sideways extending bridge is more favorable is steric hindrance. The methylene hydrogens in the 90° orientation are in very close proximity to hydrogen on the phenyl ring. In the other orientation the steric interactions of the amide hydrogen with phenyl hydrogen is considerably less. In this configuration, the bipyridine will not be able to cross link the porphyrins in the desired fashion, more likely causing aggregates when bipyridine is added.

CHAPTER 4: CONCLUSIONS

The reason for choosing TTPa as a route to synthesizing the proposed system is because the single carboxylate group provided and easy synthetic route for the creation of simple cofacial porphyrin dimer systems with an ideal site for the attachment of an acceptor. The reality of it though is that the synthesis of even a simple porphyrin dyad linked together by a carbon chain by the carboxylates proved more difficult to synthesize than expected. The production of the dyad via ester bonds proved nonviable despite several different synthetic approaches. While is certainly possible to create dyad from ester bonds as is supported by the literature[12-14, 53-54] it was decided that amides would be easier to synthesize. Creation of the dyad by creating amide bonds did prove to be more successful, but with poor yields due to side reactions. The EDC coupling has been shown to work for this system, but is perhaps not the best approach due to the poor yields. This left less time to characterize the created donor system than was needed. Only one length carbon bridge was synthesized and in a fairly low quantity.

The crosslinking studies have mixed result. There was very clear signs that coupling does occur with the addition of bipyridine in the TTP. It is a very straight forward reaction and seems to bind nearly completely based of spectroscopic evidence that shows great promise for this approach. The crosslinking reaction for the TTPa shows a very different result, with a very clear redshift in the spectroscopic data,

indicating a lack of coupling. Most importantly the dyad did not show the clear signs of the other two samples. Instead showing a very subtle redshift.

While the TTP samples show great potential for this approach. The dyad results do not show any of the desired effects. Computational and structural analysis show the reason for this to most likely be due to steric interactions of the side-bridge. This suggests that the amide bonded side bridge may not be the best approach for this system.

More work is needed before this system to determine why exactly the system failed to show signs of any coupling with a side-bridge. The hypothesis being that steric interactions are preventing the side-bridge from orienting favorably. To explore this much larger amounts of the side-bridged porphyrin must be synthesized. This would require an optimization of the EDC coupling to produce higher yields, or exploration of other means of synthesizing amides such as the reaction of amines with acyl chlorides. With a sufficient amount of the compound synthesized, it would be possible to run x-ray diffraction to determine the crystal structure and examine the preferred orientation of the side-bridge.

Likewise, side-bridges of different length chains could be synthesized for examination as well. While the best explanation seems to be steric hindrance, our calculations with an 8 carbon side chain was an exact fit, that is the inter-ring spacing in the bipyridine compex is 11.5 Å, which is the maximum size allowed by 8 carbons. It may be though that this “exact” fit for the bipyridine does not allow enough flexibility for the bipyridine to bind in the cofacial orientation. Examining the effect of longer side chains could be used to determine if this is the case.

Lastly there is the results of the temperature controlled experiments. The correlate well with the observed coupling values from the steady state experiments for TTP showing usefulness of the technique. However, the coupling shown in the data is considerably larger than the value for k_bT at room temperature. There is still room in the experimental set up to run the system to even higher temperatures and collect more data points. The use of glass forming solvents limit this though as they would boil if the temperature went too high. There is also the additional problem of the sigmoidal artifact in the lifetime data with respect to temperature that are caused by the glass transition. Converting over to film studies would eliminate the issues with the solvent in these systems.

The system design proposed by Creatore et al.[7] shows promise in its ability to create enhanced photocurrents in donor-acceptor systems without complex engineering trying to create and exploit long lived coherences. This approach to its creation in the real world remains uncertain. There are many questions still to be answered before it is clear if this approach is viable.

REFERENCES

1. Shockley, W.; Queisser, H. J., Detailed Balance Limit of Efficiency of P-N Junction Solar Cells. *Journal of Applied Physics* **1961**, *32*, 510-519.

2. Mathew, S.; Yella, A.; Gao, P.; Humphry-Baker, R.; CurchodBasile, F. E.; Ashari-Astani, N.; Tavernelli, I.; Rothlisberger, U.; NazeeruddinMd, K.; Grätzel, M., Dye-Sensitized Solar Cells with 13% Efficiency Achieved through the Molecular Engineering of Porphyrin Sensitizers. *Nat Chem* **2014**, *6*, 242-247.

3. Schlau-Cohen, G. S.; Fleming, G. R., Structure, Dynamics, and Function in the Major Light-Harvesting Complex of Photosystem Ii. *Aust. J. Chem.* **2012**, *65*, 583-590.

4. Schlau-Cohen, G. S.; Ishizaki, A.; Calhoun, T. R.; Ginsberg, N. S.; Ballottari, M.; Bassi, R.; Fleming, G. R., Elucidation of the Timescales and Origins of Quantum Electronic Coherence in Lhcii. *Nat. Chem.* **2012**, *4*, 389-395.

5. Fassioli, F.; Dinshaw, R.; Arpin, P. C.; Scholes, G. D., Photosynthetic Light Harvesting: Excitons and Coherence. *J. R. Soc. Interface* **2014**, *11*, 22.

6. Anna, J. M.; Scholes, G. D.; van Grondelle, R., A Little Coherence in Photosynthetic Light Harvesting. *Bioscience* **2014**, *64*, 14-25.

7. Creatore, C.; Parker, M. A.; Emmott, S.; Chin, A. W., Efficient Biologically Inspired Photocell Enhanced by Delocalized Quantum States. *Physical Review Letters* **2013**, *111*, 253601.

8. Barber, J., Photosynthetic Energy Conversion: Natural and Artificial. *Chemical Society Reviews* **2009**, *38*, 185-196.

9. Hayes, D.; Griffin, G. B.; Engel, G. S., Engineering Coherence among Excited States in Synthetic Heterodimer Systems. *Science* **2013**, *340*, 1431-1434.

10. Dorfman, K. E.; Voronine, D. V.; Mukamel, S.; Scully, M. O., Photosynthetic Reaction Center as a Quantum Heat Engine. *Proceedings of the National Academy of Sciences* **2013**, *110*, 2746-2751.

11. Kasha, M., Energy Transfer Mechanisms and the Molecular Exciton Model for Molecular Aggregates. *Radiation Research* **1963**, *20*, 55-70.

12. Hunter, C. A.; Sanders, J. K. M.; Stone, A. J., Exciton Coupling in Porphyrin Dimers. *Chemical Physics* **1989**, *133*, 395-404.

13. Hunter, C. A.; Meah, M. N.; Sanders, J. K. M., Dabco-Metalloporphyrin Binding: Ternary Complexes, Host-Guest Chemistry and the Measurement Of .Pi.-.Pi. Interactions. *J. Am. Chem. Soc.* **1990**, *112*, 5773-5780.

14. Hunter, C. A.; Leighton, P.; Sanders, J. K. M., Allosteric Ligand Binding to Cofacial Metalloporphyrin Dimers: The Mechanism of Porphyrin Disaggregation. *Journal of the Chemical Society, Perkin Transactions 1* **1989**, 547-552.

15. Dick, H. A.; Bolton, J. R.; Picard, G.; Munger, G.; Leblanc, R. M., Fluorescence Lifetime of 5-(4-Carboxyphenyl)-10,15,20-Tritolylporphyrin in a Mixed Langmuir-Blodgett Film with Dioleoylphosphatidylcholine - a Proposed Standard. *Langmuir* **1988**, *4*, 133-136.

16. Flamigni, L.; Talarico, A. M.; Ventura, B.; Rein, R.; Solladié, N., A Versatile Bis-Porphyrin Tweezer Host for the Assembly of Noncovalent Photoactive Architectures: A Photophysical

Characterization of the Tweezers and Their Association with Porphyrins and Other Guests. *Chemistry – A European Journal* **2006**, *12*, 701-712.

17. Flamigni, L.; Ventura, B.; Oliva, A. I.; Ballester, P., Energy Migration in a Self-Assembled Nonameric Porphyrinic Molecular Box. *Chemistry – A European Journal* **2008**, *14*, 4214-4224.

18. Anderson, H. L.; Hunter, C. A.; Meah, M. N.; Sanders, J. K. M., Thermodynamics of Induced-Fit Binding inside Polymacrocyclic Porphyrin Hosts. *J. Am. Chem. Soc.* **1990**, *112*, 5780-5789.

19. Naylor, S.; Cowan, J. A.; Lamb, J. H.; Hunter, C. A.; Sanders, J. K. M., Conformation and Electron-Transfer Chemistry in Model Photosynthetic Reaction Centres Determined by Fast Atom Bombardment Mass Spectrometry. *Journal of the Chemical Society, Perkin Transactions 2* **1992**, 411-418.

20. Hunter, C. A.; Hyde, R. K., Photoinduced Energy and Electron Transfer in Supramolecular Porphyrin Assemblies. *Angewandte Chemie International Edition in English* **1996**, *35*, 1936-1939.

21. D'Souza, F.; Deviprasad, G. R.; Zandler, M. E.; El-Khouly, M. E.; Fujitsuka, M.; Ito, O., Photoinduced Electron Transfer in "Two-Point" Bound Supramolecular Triads Composed of N,N-Dimethylaminophenyl-Fullerene-Pyridine Coordinated to Zinc Porphyrin. *J. Phys. Chem. A* **2003**, *107*, 4801-4807.

22. Kim, H.-J.; Redman, J. E.; Nakash, M.; Feeder, N.; Teat, S. J.; Sanders, J. K. M., Synthesis, Structure, and Modeling of a Cyclic Rhodium(Iii) Porphyrin Dimer with an Encapsulated 4,4‘-Bipyridine Ligand. *Inorganic Chemistry* **1999**, *38*, 5178-5183.

23. D’Souza, F.; Maligaspe, E.; Ohkubo, K.; Zandler, M. E.; Subbaiyan, N. K.; Fukuzumi, S., Photosynthetic Reaction Center Mimicry: Low Reorganization Energy Driven Charge Stabilization in Self-Assembled Cofacial Zinc Phthalocyanine Dimer−Fullerene Conjugate. *J. Am. Chem. Soc.* **2009**, *131*, 8787-8797.

24. D'Souza, F.; Chitta, R.; Gadde, S.; Rogers, L. M.; Karr, P. A.; Zandler, M. E.; Sandanayaka, A. S. D.; Araki, Y.; Ito, O., Photosynthetic Reaction Center Mimicry of a "Special Pair" Dimer Linked to Electron Acceptors by a Supramolecular Approach: Self-Assembled Cofacial Zinc Porphyrin Dimer Complexed with Fullerene(S). *Chem.-Eur. J.* **2007**, *13*, 916-922.

25. Nikolaitchik, A. V.; Rodgers, M. A. J., Crown Ether Substituted Monomeric and Cofacial Dimeric Metallophthalocyanines. 2. Photophysical Studies of the Cobalt(Ii) and Nickel(Ii) Variants. *J. Phys. Chem. A* **1999**, *103*, 7597-7605.

26. Yagi, S.; Ezoe, M.; Yonekura, I.; Takagishi, T.; Nakazumi, H., Diarylurea-Linked Zinc Porphyrin Dimer as a Dual-Mode Artificial Receptor: Supramolecular Control of Complexation-Facilitated Photoinduced Electron Transfer. *J. Am. Chem. Soc.* **2003**, *125*, 4068-4069.

27. Yagi, S.; Yonekura, I.; Awakura, M.; Ezoe, M.; Takagishi, T., Facile Synthesis of Cofacial Porphyrin Dimer and Trimer Using a Diarylurea Linkage. *Chem. Commun.* **2001**, 557-558.

28. Tranthi, T. H.; Lipskier, J. F.; Maillard, P.; Momenteau, M.; Lopezcastillo, J. M.; Jaygerin, J. P., Effect of the Exciton Coupling on the Optical and Photophysical Properties of Face-to-Face Porphyrin Dimer and Trimer - a Treatment Including the Solvent Stabilization Effect. *J. Phys. Chem.* **1992**, *96*, 1073-1082.

29. Jeong, D. H.; Jang, S. M.; Hwang, I.-W.; Kim, D.; Yoshida, N.; Osuka, A., Investigation of Interporphyrin Charge Resonance of Dihedral Angle Controlled Porphyrin Dimers by Resonance Raman Spectroscopy and Mo Approaches. *The Journal of Physical Chemistry A* **2002**, *106*, 11054-11063.

30. Takai, A.; Gros, C. P.; Barbe, J.-M.; Guilard, R.; Fukuzumi, S., Enhanced Electron-Transfer Properties of Cofacial Porphyrin Dimers through Π–Π Interactions. *Chemistry – A European Journal* **2009**, *15*, 3110-3122.

31. Tanaka, M.; Ohkubo, K.; Gros, C. P.; Guilard, R.; Fukuzumi, S., Persistent Electron-Transfer State of a Π-Complex of Acridinium Ion Inserted between Porphyrin Rings of Cofacial Bisporphyrins. *J. Am. Chem. Soc.* **2006**, *128*, 14625-14633.

32. Gros, C. P.; Brisach, F.; Meristoudi, A.; Espinosa, E.; Guilard, R.; Harvey, P. D., Modulation of the Singlet−Singlet through-Space Energy Transfer Rates in Cofacial Bisporphyrin and Porphyrin−Corrole Dyads. *Inorganic Chemistry* **2007**, *46*, 125-135.

33. Grozema, F. C.; Houarner-Rassin, C.; Prins, P.; Siebbeles, L. D. A.; Anderson, H. L., Supramolecular Control of Charge Transport in Molecular Wires. *J. Am. Chem. Soc.* **2007**, *129*, 13370-13371.

34. Ishizuka, T.; Sankar, M.; Kojima, T., Control of the Spatial Arrangements of Supramolecular Networks Based on Saddle-Distorted Porphyrins by Intermolecular Hydrogen Bonding. *Dalton Transactions* **2013**, *42*, 16073-16079.

35. Ito, F.; Ishibashi, Y.; Khan, S. R.; Miyasaka, H.; Kameyama, K.; Morisue, M.; Satake, A.; Ogawa, K.; Kobuke, Y., Photoinduced Electron Transfer and Excitation Energy Transfer in Directly Linked Zinc Porphyrin/Zinc Phthalocyanine Composite. *J. Phys. Chem. A* **2006**, *110*, 12734-12742.

36. Konarev, D. V.; Khasanov, S. S.; Slovokhotov, Y. L.; Saito, G.; Lyubovskaya, R. N., Neutral and Ionic Complexes of C60 with (Znoep)2[Middle Dot]Bpy Coordination Dimers. *CrystEngComm* **2008**, *10*, 48-53.

37. Matsui, J.; Sodeyama, T.; Saiki, Y.; Miyazawa, T.; Yamada, T.; Tamaki, K.; Murashima, T., Face-to-Face Porphyrin Moieties Assembled with Spacing for Pyrazine Recognition in Molecularly Imprinted Polymers. *Biosens. Bioelectron.* **2009**, *25*, 635-639.

38. Ring, D. J.; Aragoni, M. C.; Champness, N. R.; Wilson, C., A Coordination Polymer Supramolecular Isomer Formed from a Single Building Block: An Unexpected Porphyrin Ribbon Constructed from Zinc(Tetra(4-Pyridyl)Porphyrin). *CrystEngComm* **2005**, *7*, 621-623.

39. Stulz, E.; Scott, S. M.; Bond, A. D.; Teat, S. J.; Sanders, J. K. M., Selection and Amplification of Mixed-Metal Porphyrin Cages from Dynamic Combinatorial Libraries. *Chemistry – A European Journal* **2003**, *9*, 6039-6048.

40. Zeng, Q.; Wu, D.; Wang, C.; Lu, J.; Ma, B.; Shu, C.; Ma, H.; Li, Y.; Bai, C., Bipyridine Conformations Control the Solid-State Supramolecular Chemistry of Zinc(Ii) Phthalocyanine with Bipyridines. *CrystEngComm* **2005**, *7*, 243-248.

41. Kumar, R. K.; Diskin-Posner, I.; Goldberg, I., Solid-State Supramolecular Chemistry of Porphyrins. Ligand-Bridged Tetraphenylmetalloporphyrin Dimers. *Journal of Inclusion Phenomena* **2000**, *37*, 219-230.

42. Giovannetti, R., The Use and Spectrophotometry Uv-Vis Fo the Study of Porphyrins. In *Macro to Nano Spectroscopy*, Uddin, J., Ed. 2012; pp 87-108.

43. Gouterman, M., Spectra of Porphyrins. *J. Mol. Spectrosc.* **1961**, *6*, 138-&.

44. Gouterman, M.; Snyder, L. C.; Wagniere, G. H., Spectra of Porphyrins .2. 4 Orbital Model. *J. Mol. Spectrosc.* **1963**, *11*, 108-&.

45. Weiss, C.; Kobayash.H; Gouterma.M, Spectra of Porphyrins .3. Self-Consistent Molecular Orbital Calculations of Porphyrin and Related Ring Systems. *J. Mol. Spectrosc.* **1965**, *16*, 415-&.

46. Weaver, J. Corroles. Dissertation, California Institute of Technology, 2005.

47. Nemykin, V. N.; Hadt, R. G., Interpretation of the Uv−Vis Spectra of the Meso(Ferrocenyl)-Containing Porphyrins Using a Tddft Approach: Is Gouterman's Classic Four-Orbital Model Still in Play? *The Journal of Physical Chemistry A* **2010**, *114*, 12062-12066.

48. Little, R. G.; Anton, J. A.; Loach, P. A.; Ibers, J. A., The Synthesis of Some Substituted Tetraarylporphyrins. *Journal of Heterocyclic Chemistry* **1975**, *12*, 343-349.

49. Habdas, J.; Boduszek, B., Synthesis of Peptidyl Phosphonates Containing 5-(4′-Carboxyphenyl)-10,15,20-Tritolylporphyrin. *Heteroatom Chemistry* **2008**, *19*, 107-111.

50. Vivero-Escoto, J. L.; Vega, D. L., Stimuli-Responsive Protoporphyrin Ix Silica-Based Nanoparticles for Photodynamic Therapy in Vitro. *RSC Advances* **2014**, *4*, 14400-14407.

51. Liu, Y. H.; Anderson, J. E.; Kadish, K. M., Electrochemical Studies of Dimeric Rhodium(Iii) Porphyrins Containing a Dibasic Nitrogen-Heterocyclic Bridging Ligand. *Inorganic Chemistry* **1988**, *27*, 2320-2325.

52. Tan, R.-R.; Shen, X.; Hu, L.; Zhang, F.-S., Liquid-to-Glass Transition of Tetrahydrofuran and 2-Methyltetrahydrofuran. *Chinese Physics B* **2012**, *21*, 086402.

53. Hunter, C. A.; Sanders, J. K. M.; Beddard, G. S.; Evans, S., A New Approach to the Assembly of Electron Donor-Spacer-Acceptor Systems. *Journal of the Chemical Society, Chemical Communications* **1989**, 1765-1767.

54. Hunter, C. A.; Sanders, J. K. M., The Nature Of .Pi.-.Pi. Interactions. *J. Am. Chem. Soc.* **1990**, *112*, 5525-5534.